doi:10.1016/j.ymthe.2004.07.001

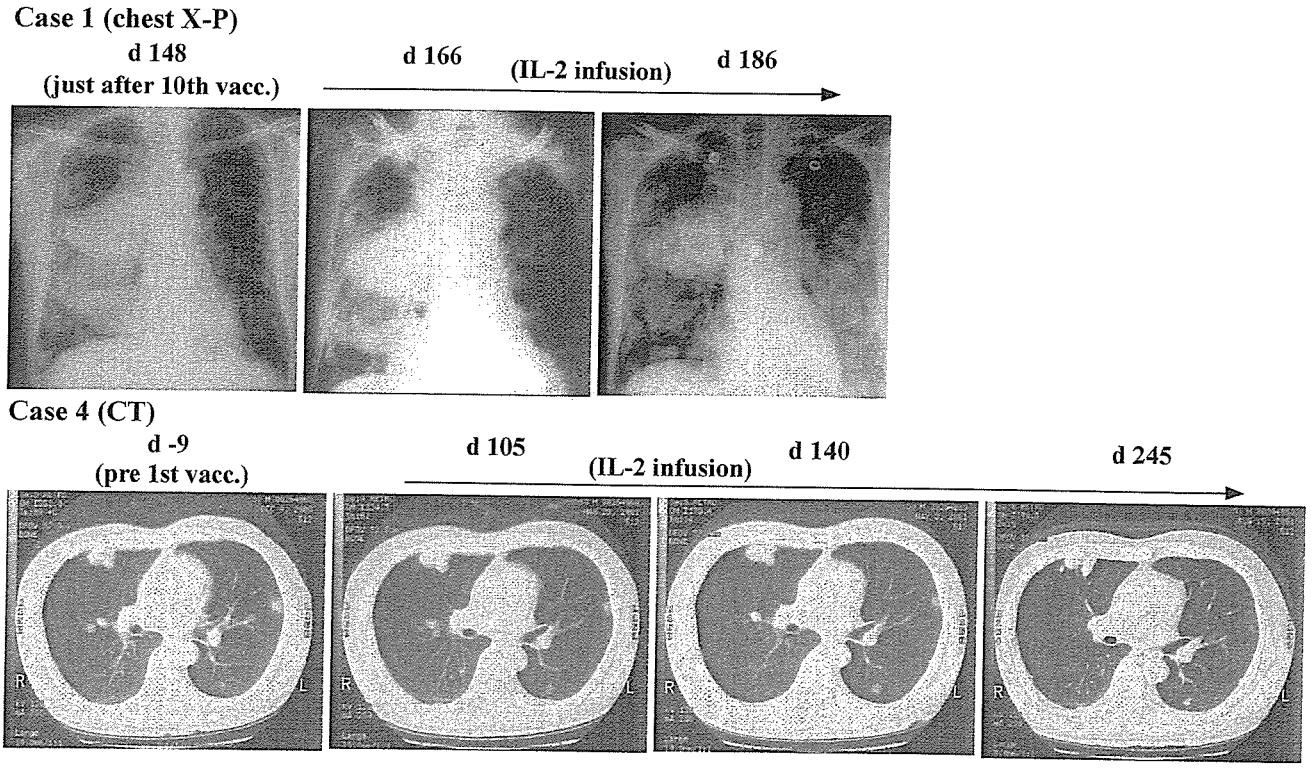

FIG. 1. Size change of the lung metastases in Cases 1 and 4 during the observation period after GVAX vaccination. (A) In Case 1, the size of the right hilar tumor, the largest metastatic lesion, became smaller after 1 week of low-dose IL-2 (d 166, day 166) and decreased by 30% after 1 month of low-dose IL-2 compared with the tumor just after the 10th vaccination. Chest X-ray films are presented. (B) In Case 4, the size of the left lung metastasis became smaller during vaccination as shown on two films for comparison between prevaccination and 105 days after the 1st vaccination. After the start of low-dose IL-2 between days 105 and 245, both the metastatic lesions in the left lung and those in the right lung became smaller. CT scan films are presented.

irradiation at a dose of 30 Gy to his femoral metastasis followed by daily low-dose rIL-2 (700,000–140,000 IU). His performance status at present, 58 months after the start of vaccination and with low-dose rIL-2 (350,000 IU) treatment, is zero.

The third patient (Case 3), a 57-year-old Japanese woman, was diagnosed in October of 1999 with RCC of the left kidney with multiple liver and lung metastases. She was nephrectomized on December 9, 1999, and the pathology showed clear cell carcinoma. She received a total of 3.2×10^8 GVAX cells in 15 subcutaneous injections, from February 22, 2000, to September 19, 2000. The adverse events she experienced during vaccination are summarized in Table 1. During the course of vaccination, the growth rate of the multiple liver tumors slowed, but the numbers and sizes of the masses did not decrease as assessed by CT scan (Fig. 2C). The sizes of the metastases in her right renal pelvis and lungs, observed on CT scan, were stable during vaccination. Her performance status was maintained at zero. After completion of the vaccination regimen, she requested systemic rIL-2 and interferon-α, but the cytokine treatments were discontinued due to the appearance of liver dysfunction, which resolved after discontinuation of cytokines. Thereafter, she received monthly LAK (lymphokine-activated killer cells) therapy, upon her request. However, her metastatic lesions gradually increased, and she ultimately died of multiple RCC metastases on November 3, 2003, 47 months after nephrectomy and 45 months after the start of GVAX vaccination.

The fourth patient (Case 4), a 50-year-old Japanese man, was diagnosed in July of 2000 with right RCC with multiple lung metastases. He was nephrectomized on September 20, 2000, and pathology showed clear cell carcinoma. He received a total of 1.4×10^8 GVAX cells in six subcutaneous injections from December 13, 2000, to February 20, 2001. The adverse events he experienced during vaccination are summarized in Table 1. During the course of vaccination, the growth rate of the largest lung tumor slowed, and several tumors disappeared or were reduced in size, i.e., a mixed response was obtained. However, the sum of all the masses was increased, as assessed by CT scan. After the sixth injection, he was found to have a metastatic brain lesion with a maximum diameter of 1 cm, and the vaccination was discontinued according to our eligibility criteria. He received gamma knife irradiation to his brain metastasis and low-dose rIL-2 (700,000–140,000 IU) was initiated, which was given

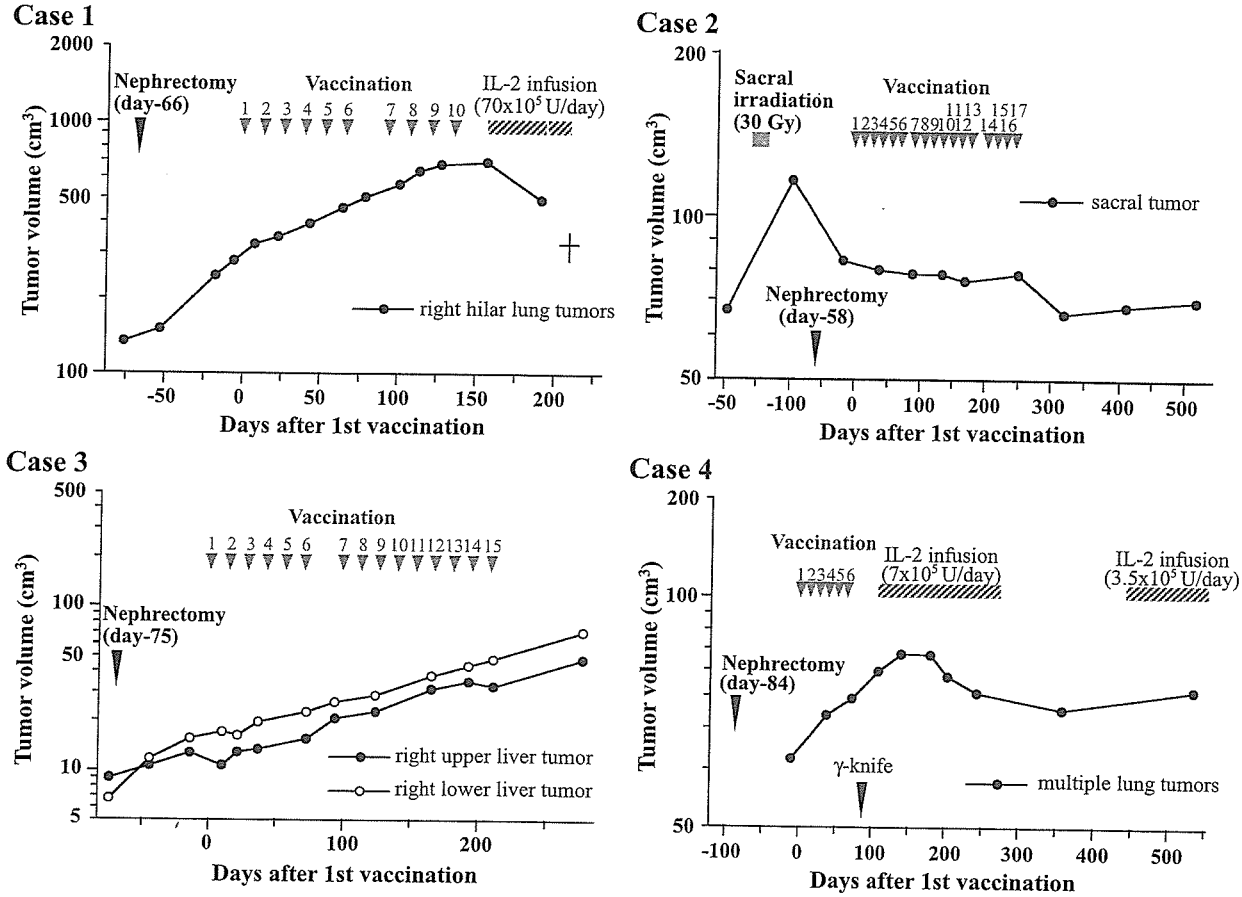

FIG. 2. Clinical summary of the four stage IV RCC patients (Cases 1 to 4) who received GVAX. The days of each vaccination are indicated by the short arrows, and the upper numbers signify the number of vaccinations. The long arrow indicates the time of nephrectomy of an RCC that involved the kidney. The tumor volume of each target metastatic lesion was measured periodically by CT scan or MRI. In Cases 1 and 4, low-dose IL-2 was administered after vaccination, upon request by the patients. The sacrum and brain were irradiated in Cases 2 and 4, respectively, to control sacral pain and brain edema.

subcutaneously, according to the patient's request. One month after the start of the rIL-2 treatment, the patient's total lung tumor volume was reduced and decreased to 30% of the peak volume over 3 months (Figs. 1B and 2D). His metastatic brain tumor was resected in January of 2002, and his performance status at present, 40 months after the start of vaccination and with low-dose rIL-2 (350,000 IU) treatment, is zero.

Autologous Vaccine Yield and Gene Transfer

In this trial, we generated the primary RCC cultures from large, advanced cancers with some areas of necrosis. The rate of successful vaccine cell expansion was 100% (6/6). In our preclinical models, the expression of paracrine GM-CSF by vaccine cells at levels higher than 40 ng/10^6 cells/24 h induced antitumor immunity, and thus, we excluded cases producing less than this level from the present study [13,14]. A single transduction with MFGS-GM-CSF generated GM-CSF secretion levels of >40 ng/10^6 cells/24 h in four of the six patients (66.6%) and their production levels are shown in Table 1. The level of GM-CSF secretion by nontransduced cells ranged from 0 to 19 ng/10^6 cells/24 h. We excluded two of the patients, who had GVAX production of only 20 and 12.4 ng/10^6 cells/24 h, respectively, from our study. Cells from these individuals incorporated fewer copies of the integrated GM-CSF cDNA, and the cell doubling times were approximately two times greater than those of the cells producing >40 ng/10^6 cells/24 h GM-CSF (data not shown). It is likely that the extended cell doubling times resulted in poor GM-CSF transduction efficiency in the two excluded cases.

Safety of Administration and Systemic Toxicities

All of the six patients' primary cultures met the vaccine cell yield specifications for at least six injections. Importantly, the tests for microbial contaminants gave negative results for all six GM-CSF-transduced products. All four patients, designated Cases 1, 2, 3, and 4, satisfied all of the eligibility criteria for this study and

doi:10.1016/j.ymthe.2004.07.001

received vaccinations (Table 1). No surgical complications were encountered that would preclude subsequent vaccination, although Case 1 had mechanical ileus 30 days after nephrectomy, which was before vaccination, and Case 2 had ileus 219 days after nephrectomy, between the 12th and the 13th vaccine injections. These symptoms were resolved by intravenous fluid replacement for several days. In the latter case, ileus was thought to be a late adverse event related to nephrectomy, but not vaccination because reinitiation of vaccination did not cause any other ileus symptoms. When vaccine yield and clinical status permitted, we performed multiple vaccinations for analysis of cumulative side effects. Cases 1, 2, 3, and 4 received GVAX at 66, 58, 75, and 84 days after nephrectomy, respectively. They received 48 fully evaluable, 14-day treatment cycles. Finally, Cases 1, 2, 3, and 4 received total cell doses of 2.2×10^8, 3.7×10^8, 3.2×10^8, and 1.4×10^8, respectively. During the vaccinations, we observed no hepatic, renal, pulmonary, cardiac, neurological, or gastrointestinal toxicities in any of the patients other than mechanical ileus in Case 2 as stated above. We observed significant increases in the numbers of peripheral blood eosinophils, but not other leukocytes, after immunization, as shown in Table 1, and the peak eosinophil level gradually increased in each case after repetitive vaccinations (data not shown). We did not observe the two most concerning toxicities, vaccine site-specific ulceration and development of acute autoimmune disease and, specifically, nephritis in uninephric patients, except in Case 4, who experienced blister formation at the vaccination site following the 6th vaccination (Table 1). We detected no RCR (replication-competent retrovirus) during the postvaccination follow-up period in any of the four patients who received the vaccine cells. The apparent lack of acute, systemic toxicity in this trial was paralleled by the lack of plasma elevation of GM-CSF in pharmacokinetic studies following treatment (data not shown). Follow-up observations for long-term toxicity, including autoimmune disease, have been under way on our two surviving patients, Cases 2 and 4, and no vaccine-related long-term toxicity has been noted to date.

Phenotype of Cells at the Sites of Vaccination

Although there was some individual variation, we noted significant infiltration by $CD4^+$ T cells and eosinophils by day 30 (after the third vaccination); Case 3 had modest eosinophilic but intense mononuclear cell infiltration throughout the course of the vaccination protocol. Thereafter, these cell infiltrations were reduced in Cases 1 and 4, but increased in Cases 2 and 3. We could detect $CD68^+$ macrophages and CD20cy-positive B cells as minor populations, but their levels were unaltered during the course of the vaccination protocol. The level of HLA-DR expression by infiltrating cells was initially low, but increased by day 30. Intradermal $S100^+$ dendritic cells were occasionally observed in most cases. These findings were comparable with previous reports [14–20].

Delayed-Type Hypersensitivity Reactions

DTH tests using Multitest CMI showed that Cases 1 and 3 had anergic scores and Cases 2 and 4 had normal scores, i.e., within the range seen for normal volunteers or patients with localized cancer (data not shown). As shown in Table 2, we did not observe significant DTH reactions (>10 mm) to unpassaged, irradiated autologous RCC cells in any of the four patients prior to treatment. Following vaccination, we observed significant DTH reactions in all patients and they were strongest after the sixth vaccination. We also observed DTH reactions to normal renal cells (NRCs), but these reactions were almost always smaller than those to RCC cells.

We examined pathological phenotypes and numerical analysis of the DTH reactions. In all four cases, significant DTH reactions against RCC were induced by days 24–28 (following the second vaccination), compared with the day 0 controls (prevaccination). $CD4^+$ T cells were more dominant than $CD8^+$ T cells at the sites of DTH reaction, followed by $CD68^+$ macrophages and a few B cells, which was a common feature of DTH in all cases. We also observed various degrees of eosinophilic infiltration with degranulation. There were no significant differences between RCC and NRC with regard to the phenotypes of the cells in the DTH reaction, although more intense cell infiltration was observed against RCC than against NRC (data not shown). Although we detected significant DTH reactions until day 133 in Case 1, we observed a certain degree of attenuation in other cases.

Immunophenotypic Analysis of Tumor-Infiltrating Lymphocytes (TILs)

We performed immunophenotypic analysis of TILs for Case 1. Immunohistochemical analysis revealed that $CD4^+$ T cells were the predominant infiltrating cell type in pretherapy primary tumors, followed by B cells (data not shown). Fig. 3 shows TILs in perivascular areas (Fig. 3A), around the foci of tumor cell apoptosis (Figs. 3B and D), and in an unremarkable area (Fig. 3D), within biopsied skin metastatic RCC specimens that were obtained 5 months after initiation of therapy. Regardless of the area under observation, the T cells in this specimen were $CD8^+$, and we detected virtually no B cells. In addition, we observed increased numbers of $CD68^+$ macrophages, especially around the apoptotic foci. In contrast to the results of the DTH test, we did not observe eosinophilic infiltration of the tumors (data not shown). Interestingly, immunophenotypic analysis of the infiltrating cells at the sites of surgically resected renal cancer and normal renal tissue, autopsied normal liver, lung, and kidney showed a predominance of

TABLE 2: Immunological findings in patients who received GVAX

	Patient 1	2	3	4
Response to DTH skin test (mm)[a]				
Prevaccination	7 × 7/6 × 4.5	0 × 0/4 × 2	3 × 6/2 × 6	0 × 0/2 × 2
Peak reaction	85 × 65/30 × 35 (6)[b]	15 × 15/10 × 10 (6)[b]	25 × 25/2 × 1 (9)[b]	17 × 11/22 × 18 (6)[b]
Lymphocyte proliferation (cpm)				
Prevaccination	5,513	5,385	1402	1550
Post third	11,637	16,486	2836	6084
Post sixth	15,845	40,578	2442	6445
Cytokine production (pg/ml)				
IFN-γ				
Prevaccination	2746	UD	50	102
Post third	4952	199	481	UD
Post sixth	3568	394	967	UD
IL-5				
Prevaccination	UD	UD	395	128
Post third	1124	UD	863	1331
Post sixth	2088	792	1850	3017
IL-10				
Prevaccination	170	UD	UD	UD
Post third	80	UD	43	254
Post sixth	235	155	130	297
Cytotoxicity assay (%)				
Prevaccination	62.8	0.2	16.0	13.0
Post third	51.4	17.0	52.9	21.0
Post sixth	45.3	27.3	36.8	27.5
TCR Vβ gene-segment repertoire analysis	PB: 9,14,15,17 TIL: 10,17,21 DTH: 10,17	PB: 1,7,10,11,21 DTH: 1	PB: 4,18 DTH and Vac: 4,7	PB: 21,23 Vac: 9 DTH: 21

UD, under the detection level; PB, peripheral blood; TIL, tumor infiltrating lymphocytes; DTH, delayed type hypersensitivity.

[a] DTH reactions were examined using cultured autologous RCC cells/normal renal cells as antigens.

[b] The numbers in parentheses show that peak DTH reactions were observed after sixth or ninth vaccination.

$CD4^+$ cells, whereas analysis at the sites of biopsied or autopsied tumor tissues obtained after vaccination or after vaccination followed by low-dose IL-2, respectively, showed a predominance of $CD8^+$ cells (data not shown).

Vaccination Enhances the Proliferative Responses and Cytokine Production Against Autologous Tumors

We assessed the cellular immune responses using the peripheral blood mononuclear cells (PBMC) of patients who received GVAX. PBMC proliferated well in response to autologous RCC cell stimulation at all times tested (Table 2). In Case 2, the proliferative response observed before vaccination was augmented after vaccination. In all cases, vaccination markedly enhanced the proliferative responses to autologous RCC in the presence of IL-2. Especially, in Cases 2 and 4, those with prolonged clinically stable disease, the proliferative responses against autologous tumor cells remained high until the end of the study (data not shown).

IFN-γ in cultures stimulated with autologous RCC was enhanced after the initial vaccinations in Cases 1, 2, and 3, but not in Case 4 (Table 2). Conversely, IL-5 and IL-10 production was enhanced after vaccination in all cases. The enhancement of IL-5 seemed to correlate with the eosinophilia observed after the sixth vaccination. We also measured IL-4 production, but the levels of this cytokine were all below the limits of detection (data not shown).

Vaccination Induces Cytotoxicity Against Autologous RCC, Allogeneic RCC, and Autologous NRC

Case 1 showed comparatively high cytotoxicity against autologous RCC before vaccination. This level was maintained until after the fifth vaccination, after which it decreased. This was consistent with the higher DTH responses against autologous RCC and NRC seen in this case (Table 2). In Cases 2, 3, and 4, vaccination increased and maintained cytotoxicity against autologous RCC (Table 2, Fig. 4). Moreover, the addition of F(ab′)2 anti-CD3 mAb efficiently inhibited cytotoxicity against autologous RCC, suggesting the involvement

doi:10.1016/j.ymthe.2004.07.001

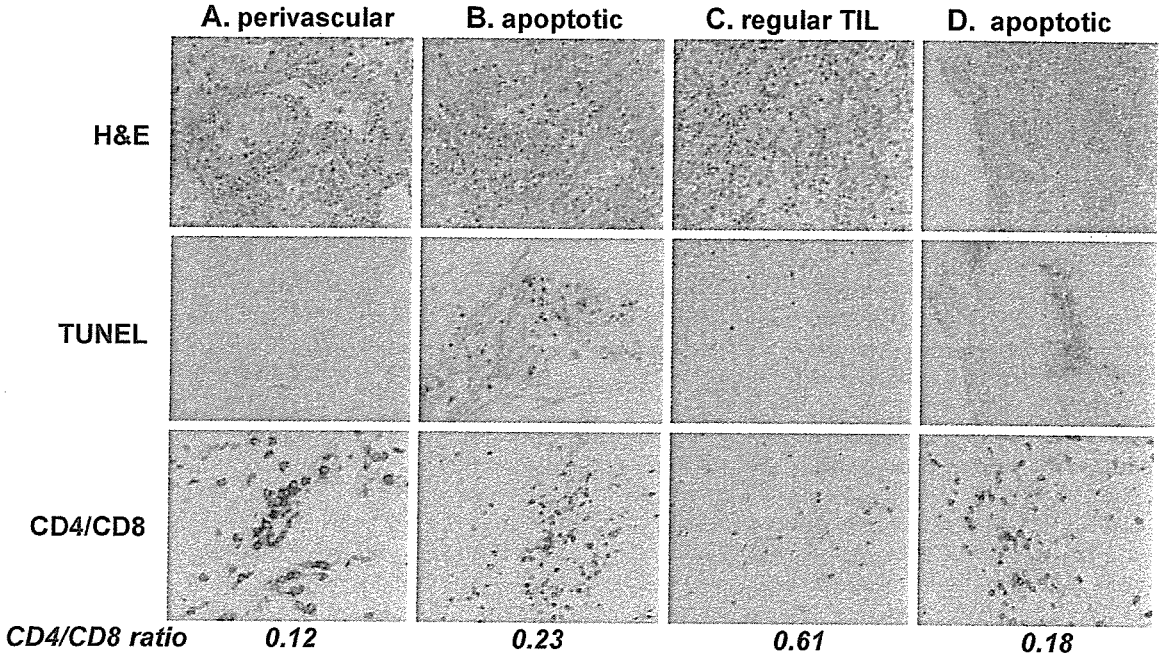

FIG. 3. Immunophenotypic analysis of tumor-infiltrating lymphocytes (TILs) in the RCC tumors of Case 1. TILs were observed in various areas, particularly (A) in the perivascular area, (B, D) around foci of tumor cell apoptosis, and (C) in unremarkable areas, within metastatic RCC that were obtained 7 months after the initiation of therapy. The T cell phenotype in this specimen had been converted to CD8 dominant, and few B cells were detected. To detect tumor apoptosis, the TUNEL method was applied as described under Patients and Methods.

FIG. 4. Cytotoxicity against autologous RCC in Cases 1 to 4. PBMC were cultured with irradiated GM-CSF-transduced autologous RCC in the presence of IL-2 for 7 days in 96-well microplates and ^{51}Cr-labeled target cells were added. After a 6-h incubation, cytotoxicity was measured as described under Patients and Methods. Asterisks in the panels for auto-RCC targets show the cytotoxicity, which was inhibited by more than 25% by the addition of F(ab')2 anti-CD3 mAb. Additional experimental values (squares) assessing the long-term results with additional treatment after the last vaccinations are also shown. IL-2, the rectangular bar represents the period of the administration of low-dose IL-2; R; γ-knife, gamma knife treatment was done for brain metastasis before the administration of IL-2.

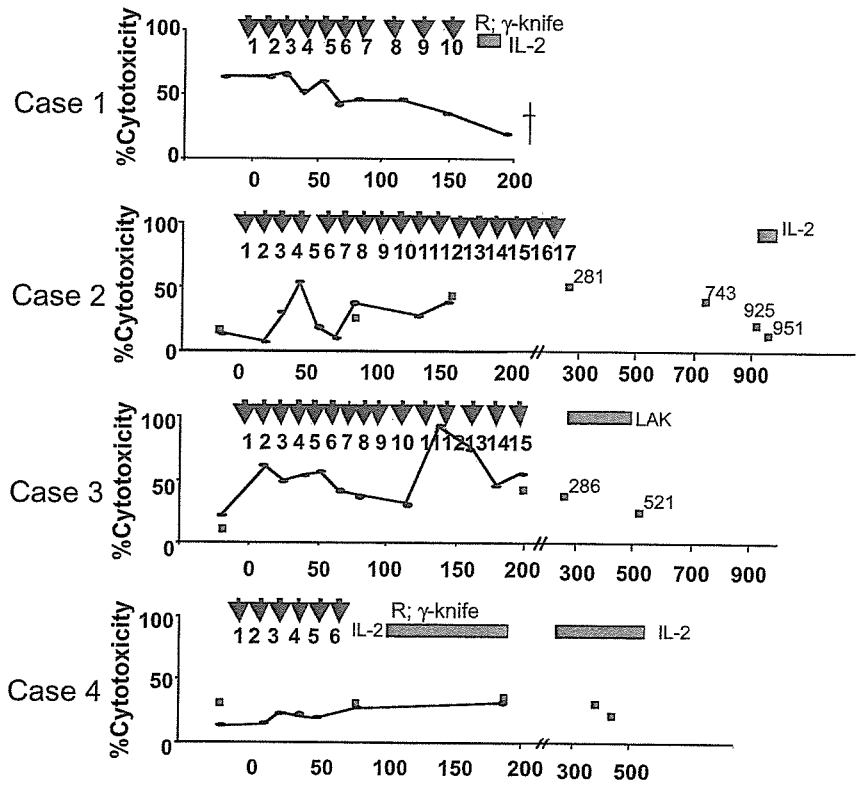

of MHC-restricted T cell receptor (TCR)-mediated cytotoxicity.

TCR Vβ Clonotypic Analysis in DTH, Lung Metastasis, and RCC

In Case 1, we analyzed TCR Vβ gene usage in peripheral blood lymphocytes (2 days before vaccination and after the 6th and 9th vaccinations) and in tumor-infiltrated lymphocytes collected from tissue samples from the original surgically resected tumor, DTH skin biopsy (biopsied after the 4th vaccination), a metastatic skin lesion (biopsied after the 10th vaccination), and autopsied right hilar main lung metastases. We estimated the variation in the signal intensity by comparing the ratio of each Vβ signal observed in the regressed metastasized lung lesion with that observed in the nonregressed lung lesion or at the biopsied RCC or NRC DTH sites. The Vβ repertoire, which was overexpressed in the former sample, but not in the latter, was considered to indicate strong candidate T cell clones that were specifically induced by GVAX. In Case 1, we observed oligoclonal expansion of T cells with Vβ 9, 14, 15, and 17 repertoires in peripheral lymphocytes after the 9th vaccination (Fig. 5A). T cells with Vβ 10, 17, and 21 repertoires infiltrated the regressed tumor to a greater extent than the nonregressed tumor. These cells were also observed in the metastatic skin lesion (Fig. 5B). Interestingly, after vaccination, T cells with Vβ 10, 17, and 21 repertoires expanded clonally in the peripheral blood of Case 1, and the amplified TCR exactly matched those of the amplified fragments in a tumor-specific manner, namely T cells with Vβ 10 expanded dominantly in original tumor and lung metastasis, T cells with Vβ 17 in lung metastasis and much less in original tumor, and T cells with Vβ 21 in arm and lung metastasis and less in original tumor (Fig. 5C).

In Case 2, a T cell clone with Vβ 1 was increased in the pre- and postvaccination peripheral blood, nephrectomized tumor, biopsied sacral tumor, and DTH sites (Table 2). We saw oligoclonal expansion of T cells with Vβ 7, 10, 11, and 21 in peripheral lymphocytes after the vaccinations. Among them, T cell clones with Vβ 10, 11, and 21 expanded gradually after the first vaccination, and those with Vβ 7, 11, and 21 were also found in the nephrectomized original tumor.

In Case 3, the number of peripheral blood T cells with Vβ 18 was increased after the 6th, 9th, and 11th vaccinations and those with Vβ 4 were increased only after the 1st vaccination. Interestingly, T cells with Vβ 4 and 7 were increased at the RCC DTH sites after vaccination. These cells were also found at the vaccination site. T cells with Vβ 4 also infiltrated the metastasized liver tumor and nephrectomized original tumor.

In Case 4, peripheral lymphocytes contained increased numbers of T cells with Vβ 23 after the vaccinations. T cells with Vβ 9 were expanded after the sixth vaccination at the vaccinated site. T cells with Vβ 21 were expanded at the RCC DTH sites. The results of the T cell repertoire analysis are summarized in Table 2.

Western Blotting

To examine whether the therapeutic regimen induced antitumor antibody responses in patients, we compared the serum antibody reactivity against autologous tumor cell lysates before and after initiating the therapy by immunoblot analysis. Using posttherapy serum as probes, high-molecular-weight proteins of around 250 kDa generated clear signals, whereas the pretherapy serum showed no or only weak signals at the same position (Fig. 6A), suggesting that the GVAX induced an antibody response in Cases 1, 2, and 4, while the results were less clear in Case 1. The signals appeared in similar positions in all patients, suggesting the presence of common antigens. These high-molecular-weight antigens were present in both tumor lysates and NRC lysates (Fig. 6A). In addition, human lip-derived fibroblasts might have identical antigens, while H69 lung cancer cells did not (Fig. 6B). Furthermore, the changes in the magnitude of the antibody immunoreactivity over time were analyzed using serum from Case 2. The strongest signal was observed in serum obtained 67 days after the initial vaccination, between the 5th and the 6th vaccinations. This response was maintained from day 67 until day 281, just after the 17th vaccination, and the immunoreactivity remained until the last time point examined at day 950 (Fig. 6C).

Clinical Outcomes

According to the standard clinical criteria, Case 2 was in stable disease, Case 4 was in mixed response, and Cases 1 and 3 were in progressive disease during the course of GVAX treatment (Table 1). As described under Case Presentations, Case 1 and Case 3 died of multiple metastases 7.5 and 45 months, respectively, after the first vaccination. Case 2 and Case 4 are alive 62 and 44 months, respectively, after the first vaccination in a stable condition with a performance status of zero. Interestingly, Case 1 with progressive disease and Case 4 with mixed response showed 30% decreases in their main or total lung metastatic lesions, respectively, 1 to 3 months after the start of low-dose IL-2 treatment (Figs. 2A, B, and 4).

DISCUSSION

Although the production of the GVAX from all six patients was successful, in two cases the levels of GM-CSF produced were not high enough for cell injection. Our production rate of 67% was compatible with previous reports [14–16]. The poor transduction efficiencies in our two patients were probably due to slowed proliferation of these RCC cells, as reflected by the extended doubling times. To overcome the heterogeneous transduction efficiency with retroviral vectors,

doi:10.1016/j.ymthe.2004.07.001

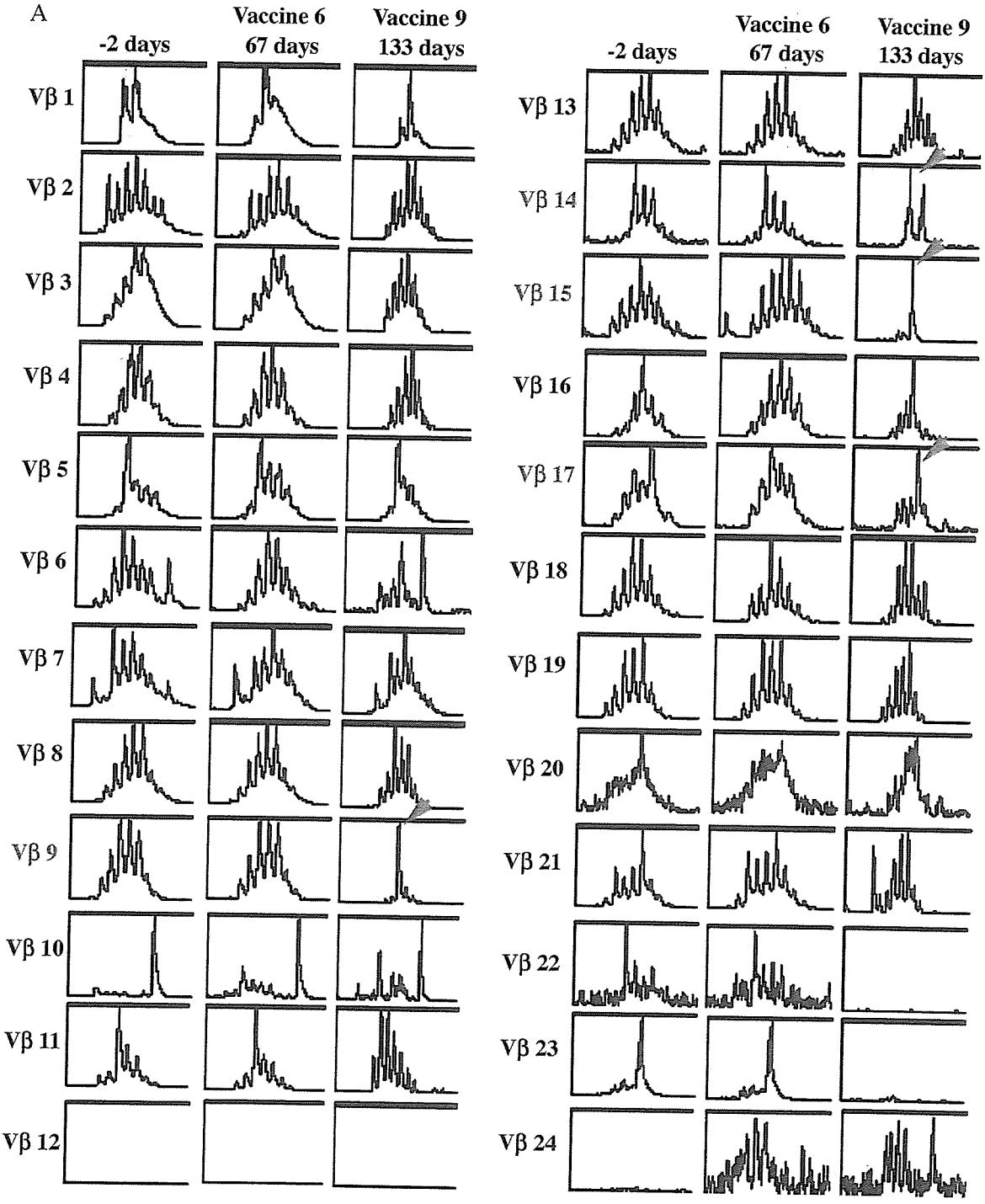

FIG. 5. TCR Vβ clonotypic analysis of the T cell infiltration in DTH, lung metastasis, and renal cell carcinoma in Case 1. (A) Oligoclonal expansion of T cell Vβ 9, 14, 15, and 17 repertoires was observed in peripheral lymphocytes after the ninth vaccination. (B) Larger numbers of T cells with Vβ 10, 17, and 21 repertoires infiltrated the regressed tumor than the nonregressed tumor. These cells were also observed in the skin metastasis designated Arm Meta. (C) After vaccination, T cells with Vβ 10, 17, and 21 repertoires were clonally expanded, and the amplified respective Vβ fragments exactly matched those of the amplified fragments in a tumor-specific manner.

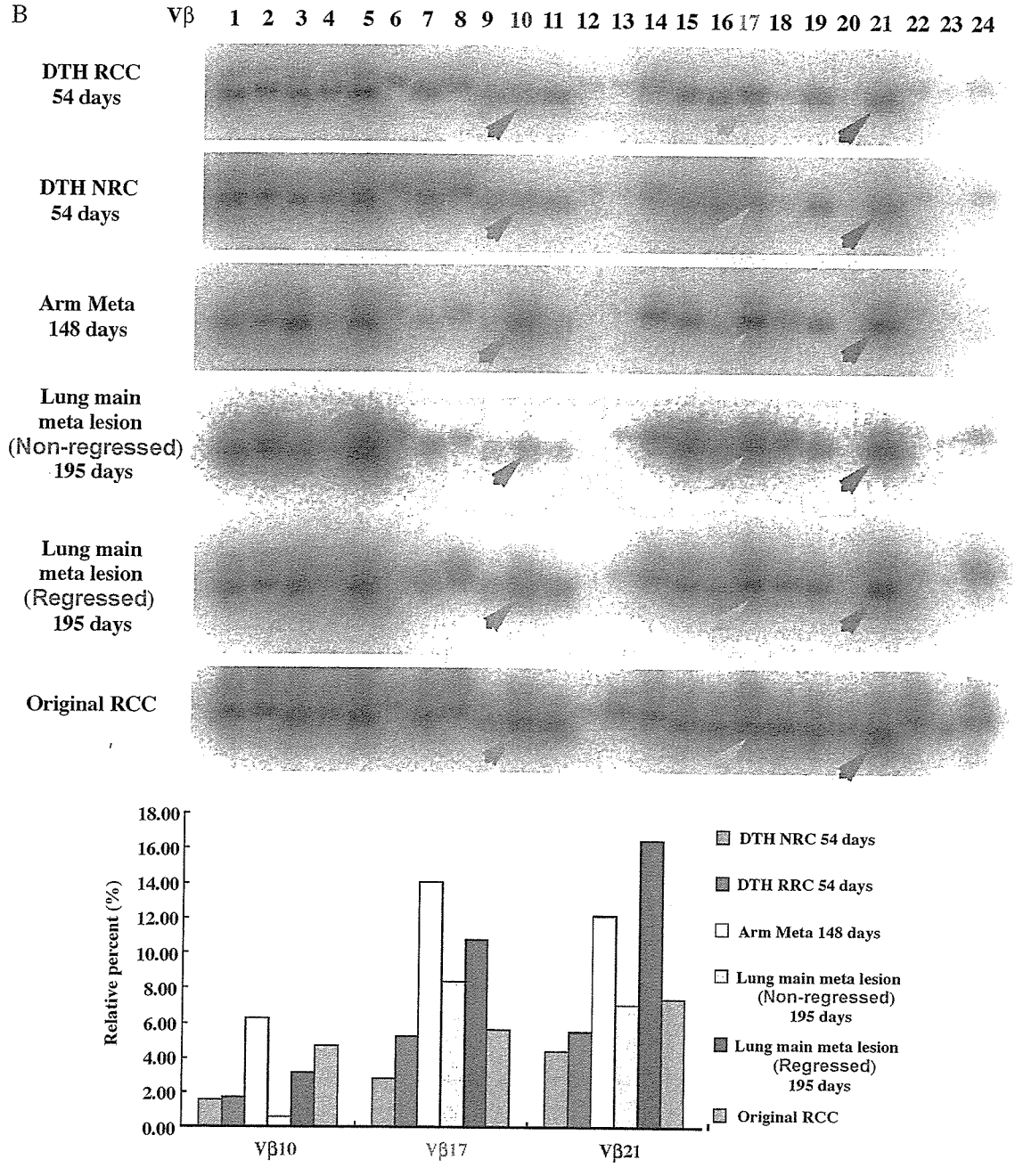

FIG. 5 (*continued*).

adoption of adenovirally transduced GM-CSF autologous tumor cells, allogeneic GM-CSF-transduced cell lines, or autologous tumor cell-based vaccines using GM-CSF-producing bystander cells should be examined as suggested previously [18–20,25–27].

We administered GVAX to four postnephrectomy patients with stage IV RCC without inducing severe vaccine-related adverse events. Furthermore, no remarkable long-term adverse events have been observed in three patients, including two living patients. Our histological findings at the vaccination sites also support the previous observations of triggering the antitumor immune response at these sites [12,14–20,28]. DTH responses in Cases 1, 2, and 3 tended to show stronger reactions to autologous RCC cells than autologous NRC and suggested that anti-RCC-specific immunity was

doi:10.1016/j.ymthe.2004.07.001

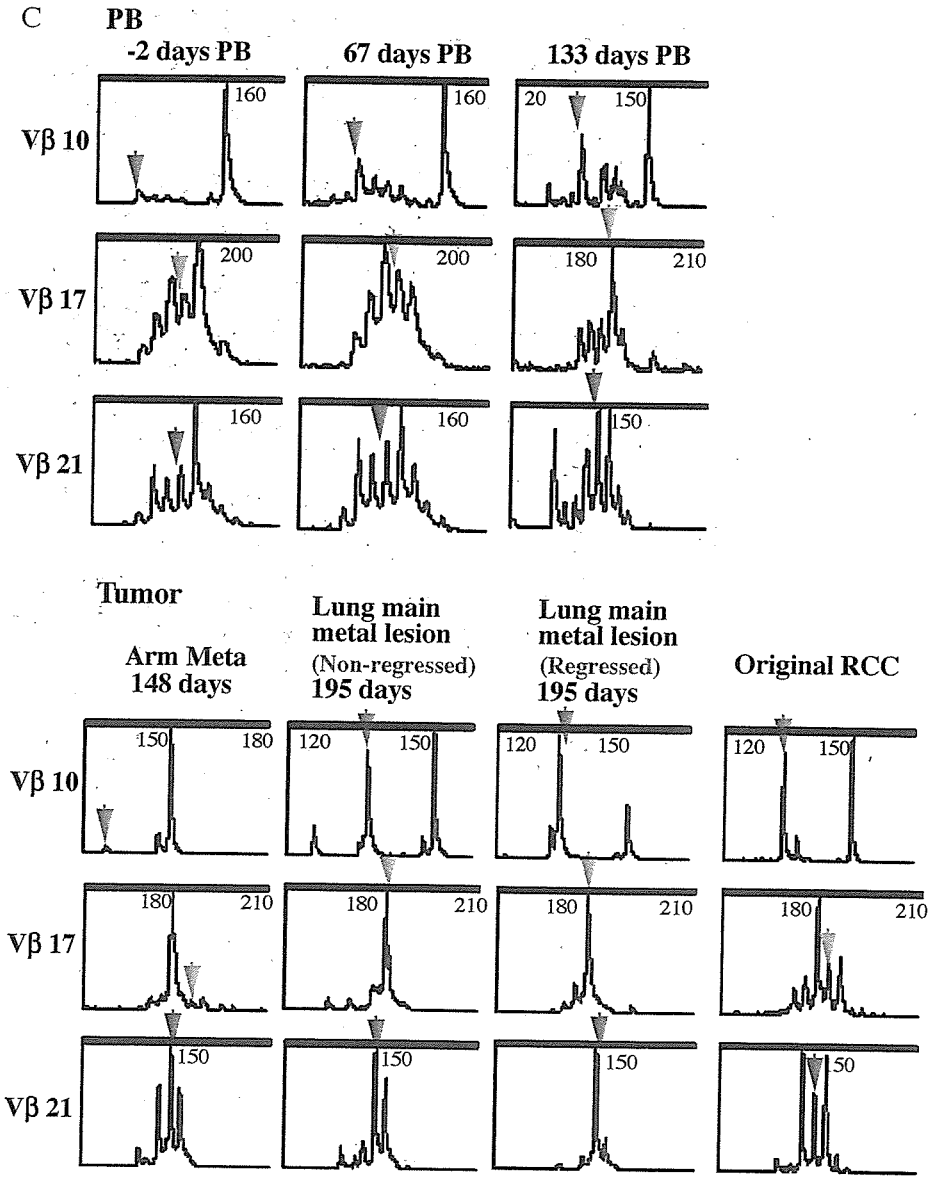

FIG. 5 (*continued*).

induced in these patients. Conversely, the reactions were also positive for NRC, most notably in Case 4, as judged by the skin reaction size (Table 2). The possible causes for this strong background DTH reaction include minimally residual xenoproteins of collagenase or trypsin in GVAX [14] and unknown common antigens existing between NRC and RCC, as the cells that infiltrated into the vaccination sites of RCC and NRC were phenotypically identical, although the number of the former cells was more prominent (data not shown). Thus, possible adverse events of autoimmune nephritis should be monitored carefully. Our follow-up observations over 3 years showed no remarkable renal dysfunction in Cases 2, 3, and 4. Also, Case 1 had no pathological changes associated with autoimmune nephritis in autopsy specimens 7 months after the vaccinations (data not shown). This long-term observation might support the safety of GVAX and its capability of inducing anti-RCC-specific immunity.

The significance of our effector-phase pathological analysis should be emphasized. We had a chance to

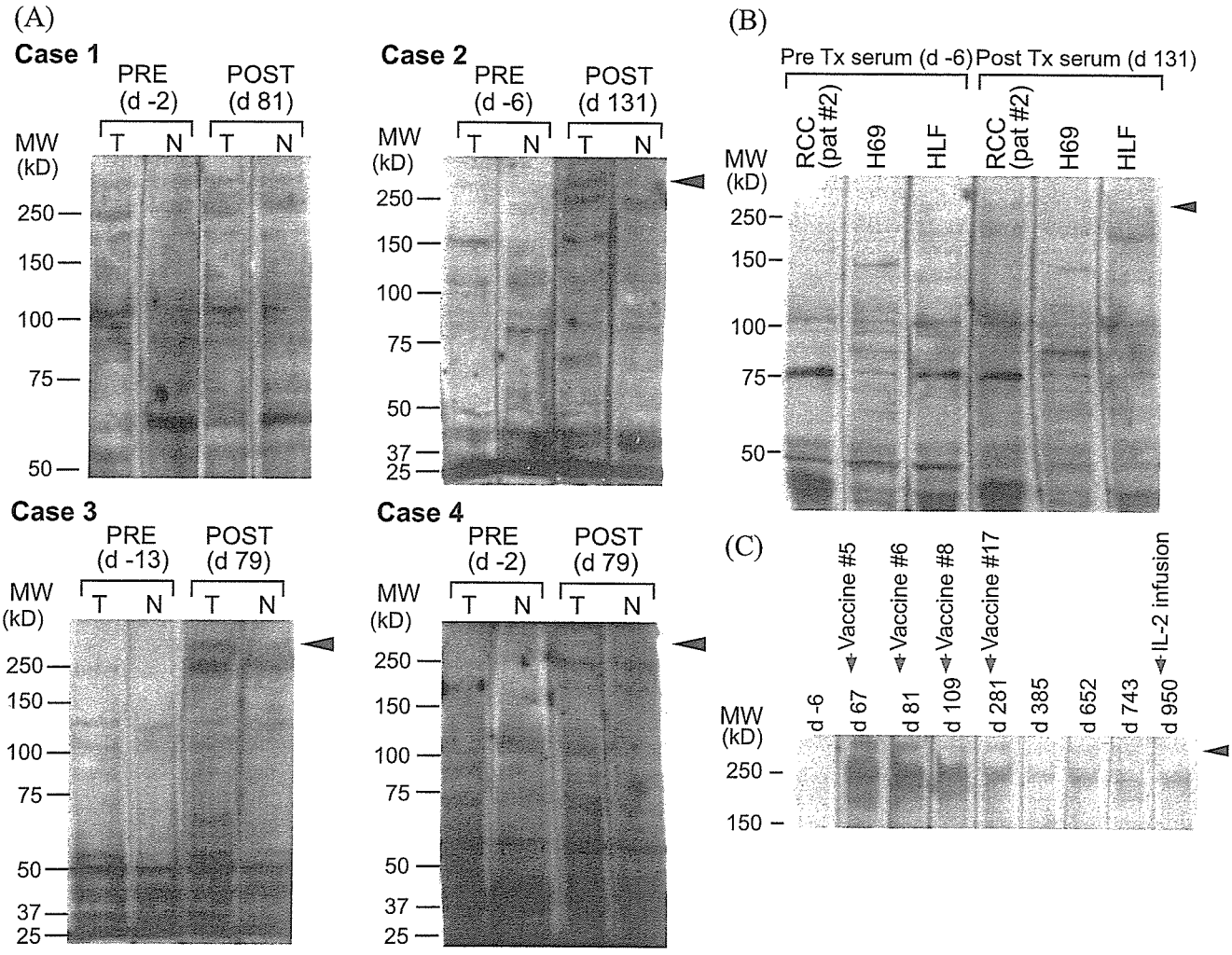

FIG. 6. Appearance of antitumor antibody responses in Cases 1 to 4, who received GVAX. (A) Comparisons of serum reactivity to autologous RCC proteins pre-GTx and post-GTx. Proteins extracted from cultured tumor cells (lane T) or normal kidney cells (lane N) were electrophoresed, transferred onto PVDF membranes, and detected with autologous patient sera (Cases 1 to 4). Sera were harvested before (PRE) and after (POST) the first vaccination (day 0). (B) Comparison of the serum reactivity to autologous RCC, H69 cells, and human lip fibroblasts (HLF). The reactivity to high-molecular-weight proteins was significant in autologous RCC and HLF, while it was weak in H69 cells. Autologous RCC from Case 2 (pat #2) was used. (C) Time course of changes in serum reactivity to high-molecular-weight proteins of approximately 250 kDa in Case 2. Immunoblotting of RCC proteins from Case 2 with autologous sera harvested at several postvaccination days (post-5th, 6th, 8th, and 17th vaccination and before the administration of low-dose IL-2).

investigate pathologically the RCC before and after vaccinations in Case 1 and have demonstrated the induction of tumor site-specific infiltration of predominantly $CD8^+$ T cells. This was associated with tumor apoptosis in postvaccinated biopsy and autopsy tumor specimens, whereas $CD4^+$ T cells predominated and tumor cell apoptosis was negligible in the original RCC (Fig. 3). Notably, these changes were demonstrated in the biopsy specimen that was obtained before IL-2 administration. These observations strongly suggest the induction of tumor-specific immunity by GVAX. Although GVAX could induce both the localization of $CD8^+$ cells within metastatic tumors and significant apoptosis, not all of the tumors showed regression. Thus, GVAX-induced antitumor immunity per se may not be sufficient for clinical efficacy.

We studied various parameters, as it is still unknown which immune factors can be used to predict the therapeutic efficacy of antitumor immune gene therapy. The results of our *in vitro* assessment of cytokine production were compatible to those reported by Soiffer *et al.* [13]. These cytokine profiles indicated the coordinate expression of gene products associated with both Th1 and Th2 cells and suggested that multiple lymphocyte effector mechanisms contribute to the potent antitumor immune response. The cytokines produced by

doi:10.1016/j.ymthe.2004.07.001

these $CD4^+$ T cells activate eosinophils, as well as macrophages that produce both superoxide and nitric oxide. Both of these cell types then collaborate at the site of the tumor challenge to cause its destruction [13]. Our observation suggested that this Th2-dominant immunological response was particularly enhanced, namely, an *in vivo* immune shift from Th1 dominance to Th2 dominance was induced after repeated vaccinations and maintained. Previous studies of GM-CSF immune gene therapy assayed cytotoxicity using PBMC or TIL [13–15]. Kusumoto *et al.* reported that vaccination with irradiated autologous GM-CSF-producing melanoma cells appeared to increase the cytotoxicity against autologous tumor cells in five patients, although repeated vaccination appeared to decrease the CTL activity in two of these cases. They suggested that vaccination of these patients with autologous melanoma cells caused T cell anergy or tolerance [14] without demonstrating the precise underlying immune mechanism involved. In the present study, Case 1, with large lung metastases, which might have contributed to the observed immunological suppression, showed similar results. Although cytotoxicity assayed using PBMC gradually decreased in Case 1, our pathological findings in the metastatic lesion showed the predominant infiltration by CD8 T cells. These findings might support the limited predictability of the *in vivo* antitumor reaction using only traditional immunoassays using PBMC.

Recently, T cell receptor β chain repertoire analysis methods were reported to facilitate the detection of clonal T cell expansion in various biological specimens. As RCC is thought to be a tumor whose growth may be controlled by the immune response, characterization of T lymphocytes found in RCC patients may demonstrate this important issue [16,17]. Using CDR3 length pattern analysis, Puisseux *et al.* demonstrated a selective localization of oligoclonal T cell populations in malignant tissues after comparisons to the T cell repertoire in the tumor and in the autologous peripheral blood lymphocytes or normal adjacent kidney [16]. Importantly, in our clinical studies, the induction of oligoclonal expansion of T cells with the selected TCR in the peripheral blood, skin biopsy specimens from DTH sites, and tumors was demonstrated after vaccination. The reasons for the observed different clonal T cell expansions in the different tissues in our studies may arise from either a polymorphic T cell response to the same antigen or a different immunogenic environment [17]. Hanada *et al.* recently demonstrated the important role of posttranslational protein splicing in the immune recognition of self and foreign peptides using human RCC antigens, and this phenomenon may explain our results [29]. Although we could not prove directly that these oligoclonally expanded T cells responded to RCC antigens, our findings of the generation of MHC-restricted and TCR-mediated cytotoxicity against autologous RCC and the predominant infiltration of CD8 T cells and apoptosis in metastatic lesions [1] supported this possibility.

In addition to the enhanced antitumor cellular immunity, GVAX is thought to induce antitumor humoral immunity. Simons *et al.* measured increased titers of antibodies recognizing prostate tumor antigens in sera from patients vaccinated with GM-CSF-transduced autologous prostate tumor cells. New antibodies recognizing polypeptides of 26, 31, and 150 kDa in extracts from LN CapPCA cells were observed in three of eight patients following the final vaccinations [18]. Soiffer *et al.* reported similar observations, with antibodies recognizing different polypeptides, in melanoma patients [13]. In the present study, Western blot analysis identified RCC-derived polypeptides of 65 and 250 kDa. We are currently screening RCC cDNA expression libraries with our patients' sera using the SEREX method to look for RCC-specific antigens other than RAGE and G250 [30,31]. We have already cloned several candidate cDNAs and are studying their RCC specificities and the possibility of their future application in anti-RCC immunotherapy.

Currently, several candidate strategies to enhance the systemic anti-RCC immunity of GVAX can be considered. These include the coadministration of IL-2 to enhance basal antitumor immunity [3,5–7,32–34], allogeneic stem cell transplantation, including nonmyeloablative stem cell transplantation to introduce allogeneic immunity [27], IL-12 or CD80 cDNA-transduced autologous tumor cells for the direct activation of CTLs, the blockade of CTLA-4/B7 interactions with monoclonal antibody to activate costimulation signals, and the functional activation of dendritic cells using HSP gp91 [35–38]. The administration of low-dose IL-2 as an anticancer immunotherapy has recently been introduced to decrease both the side effects and the cost of treatment [39–42].Our experience with three patients who were given GVAX followed by low-dose IL-2 would cast new light on anti-cancer immunotherapy, possibly by inducing tumor-specific immunity by GVAX, followed by enhancement of the broad antitumor immunity with systemic low-dose IL-2. In the present study, *in vitro* CTL analysis in these two patients supported the hypothesis that the antitumor CTL activity was maintained after administration of IL-2. The optimal duration of treatment with low-dose IL-2 in combination with GVAX remains to be determined by closely monitoring antitumor immunity both *in vitro* and *in vivo*.

PATIENTS AND METHODS

Selection of Patients

The details of the study design and methods of vaccine production were essentially the same as those reported by Simons *et al.* [13,14], except for modifications that were implemented according to the regulations for

clinical gene therapy announced by the Japanese government between 1995 and 1997. Briefly, patients with stage IV RCC (Union Internationale Contre le Cancer classification of 1997) were eligible. Chemotherapy, radiotherapy, systemic IL-2- or interferon-α-based regimens, or other investigational agents were also offered as treatment options to these patients. The following eligibility criteria were used: primary RCC in place with evaluable metastasis after nephrectomy; Eastern Cooperative Oncology Group performance status of zero or one; appropriate surgical candidate and estimated life expectancy of at least 6 months; no major surgery, radiotherapy, chemotherapy, immunotherapy, or immunosuppressive medications within 1 month prior to enrollment; age >18 years; absence of active infection, i.e., WBC count <4000/μl, platelets <100,000/μl, total bilirubin <1.5 mg/dl, and creatinine <2.0 mg/dl; HIV seronegativity; and no history of autoimmune disease. The exclusion criteria included age <20 years; pregnant or lactating women; double malignant tumors; surgery; local or systemic treatment with corticosteroids; immunotherapy; irradiation or anti-cancer drugs 1 month before registration; leukocytosis of unknown origin; history of systemic lupus erythematosis, sarcoidosis, rheumatoid arthritis, autoimmune hemolytic anemia, autoimmune thyroiditis, glomerulonephritis, or vasculitis; apparent infection requiring treatment before second stage; apparent brain metastasis detected on CT scan or MRI; postnephrectomy deep vein thrombosis or pulmonary embolism that required treatment; and opium or alcohol abuse. The study was reviewed and approved by the Committee on Clinical Investigation and Institutional Gene Therapy Ethical Committee, The Institute of Medical Science, University of Tokyo, in April 1998, and by the Joint Committee of the BioScience Committees of the Ministry of Health, Labor, and Welfare and the Ministry of Education, Culture, Sports, Science, and Technology in August 1998.

Study Design

Patients were enrolled from September 1998 to May 2001. Eligible patients were nephrectomized after giving their initial informed consent. The second informed consent was obtained after safety confirmation tests, which included negative tests for microbial contaminants such as bacteria, fungi, mycoplasma, RCR, and endotoxin, and when sufficient production (>40 ng/10^6 cells/24 h) of GM-CSF was detected in the GM-CSF gene-transduced RCC. The vaccination schedule of GVAX, including additional vaccinations, is described precisely under Vaccine preparation and administration. Peripheral blood was obtained (as per NIH Recombinant DNA Advisory Committee and Food and Drug Administration guidelines) for detecting RCR before treatment, after vaccination, monthly for 3 months, every 3 months for the next 9months, and then yearly [14]. Long-term follow-up, including periodic evaluation for autoimmune disease and tumor progression, was performed.

Clinical Evaluation

The patients received daily physical examinations and periodic laboratory tests, which included hematological parameters and liver, renal, and immunological functions, prior to and after the vaccinations. The metastatic lesion volumes were measured using CT (lung, liver, bone, brain), MRI (liver, bone, brain), and thallium or technetium scintigraphy (whole body). Unenhanced helical CT images that covered each lesion were obtained during a single breath-hold. The thickness of the slices ranged from 3 to 10 mm, depending on the lesion size. The data were transferred to a workstation (Advantage Windows; General Electric Medical Systems, Milwaukee, WI, USA) to calculate the tumor volumes. Low-density areas, which represent lung parenchyma, were excluded at a threshold of −400 HU, and lesion sections were selected manually from the remaining areas of each slice. The lesion volume was calculated with a 3-D utility on the workstation for Cases 1, 2, and 3. The lesion in Case 4 was calculated as the sum of the perpendicular diameters of all lesions measured by CT scan, due to difficulties in measuring small multiple tumors volumetrically.

Vaccine Preparation and Administration

The methods used for autologous RCC vaccine preparation and MFGS-GM-CSF gene transfer at the Clinical Cell Processing Facility of the Institute of Medical Science Hospital at the University of Tokyo have been described previously [13]. The procedure complied with good manufacturing practices. Primary cultures were established and transduced at the first passage. Following *in vitro* expansion, the vaccine cells were irradiated at 150 Gy to prevent clonogenic survival *in vivo* after vaccination. GM-CSF production was determined using a GM-CSF ELISA kit (R&D Systems, Minneapolis, MN, USA) according to the manufacturer's instructions. Genomic integration of the GM-CSF cDNA into the patients' autologous RCC cells was determined by the standard Southern blotting method using MFG-GM-CSF plasmid DNA to determine the copy number, as described elsewhere [43]. The tests for microbial contaminants, i.e., bacteria, fungi, mycoplasma, RCR, and endotoxin, were all performed by BioReliance Corp. (Rockville, MD, USA). The vaccine cells were stored in liquid nitrogen until use. On the day of vaccination, 4×10^7 viable cells were administered intradermally in the first injection, and thereafter, 2×10^7 cells were administered at least five times at 2-week intervals, which was considered to be a superior vaccination schedule as described by Soiffer *et al.* [16]. Each patient was carefully screened for eligibility according to the inclusion criteria by the Institutional Review Board (IRB) of the Institute of Medical Science, University of Tokyo. The IRB permitted additional

doi:10.1016/j.ymthe.2004.07.001

administration of vaccine every 2 weeks when the yield of cells was higher than the 1.4×10^8 cells required for the six scheduled administrations and in cases in which the patient's physical condition was acceptable after further informed consent was obtained. The vaccinated sites were biopsied for microscopic examination at 3 and/or 7 days after every second vaccination.

Toxicity Assessment and Pharmacokinetic Analysis of Serum GM-CSF Levels

The levels of toxicity were graded using the National Cancer Institute's cancer common toxicity criteria for clinical trials. Toxicities were identified by medical history, physical examination, and review of the laboratory studies performed. Patients' sera were frozen in 1-ml aliquots at −80°C until the day of testing. The serum GM-CSF levels were determined for all collection time points by enzyme-linked immunosorbent assay using the Biotrak human GM-CSF ELISA system (Amersham International Plc., Amersham, UK) according to the manufacturer's protocol.

Histological Studies

Six-millimeter punch biopsies were removed from the intradermal injection sites on days 3 and/or 7 following the first vaccination. Prevaccination skin biopsies were obtained for comparison. Similarly, skin biopsies were also taken for evaluation of the DTH reaction 48 h after intradermal inoculation of RCC cells and NRC. Surgically removed and autopsy materials were used for the histological evaluation of tumors and tumor-infiltrating cells. Biopsy materials were fixed in 10% buffered formalin, embedded in paraffin, stained with H&E, and labeled with antibodies to CD3, BMP (rabbit antiserum to human myelin basic protein; DAKO Corp., Carpinteria, CA, USA), AE1/AE3 (pooled mAbs to human epithelial keratin, IgG1 subtype; Boehringer Mannheim, Indianapolis, IN, USA), S100 (rabbit anti-cow S100; DAKO), CD68 (anti-human macrophage CD68 mAb, IgG3-subtype; DAKO), HLA-DR (clone LN3, IgG2a subtype; Lab Vision Corp., Fremont, CA, USA), CD3 (clone PS1, mAb, IgG2a subtype; Novocastra Laboratories, Newcastle, UK), CD4 (clone 1F6, mAb, IgG1 subtype; Novocastra Laboratories), CD8 (clone 1A5, IgG1 subtype; Novocastra Laboratories), and CD20cy (B cell marker, clone L26, mAb, IgG2a subtype; Lab Vision Corp.). For the evaluation of tumor apoptosis, the TdT-mediated dUTP–biotin nick end-labeling (TUNEL) method was applied using an ApopTag Kit (Intergen Co., Purchase, NY, USA).

Delayed-Type Hypersensitivity Testing

To evaluate the cell-mediated immunity status of each patient before and after treatment, DTH testing was performed using seven common recall antigens (Multitest CMI; Connaught Laboratories, Swiftwater, PA, USA) according to the manufacturer's instructions. Reaction scoring was also performed according to the manufacturer's instructions. The patients were tested simultaneously for reactivity to autologous, irradiated cultured RCC cells and NRC. The autologous RCC cells and NRC for DTH testing were prepared and stored in liquid nitrogen according to the same procedure used for vaccine cell production omitting GM-CSF transduction. During storage, sterility testing for bacteria, fungi, mycoplasma, and endotoxin was carried out at the Department of Laboratory Medicine, Institute of Medical Science, University of Tokyo. PBMC were isolated using the standard Lymphoprep (d = 1.077; Nycomed Pharma AS, Oslo, Norway) density gradient centrifugation method. These cells were washed three times with HBSS, counted, and injected intradermally at 10^6 cells/0.2 ml. DTH reactions were observed 48 h after each DTH injection, i.e., 1 week before the first vaccination and 1 week after the second, fourth, and sixth vaccinations in all four patients.

Tumor Tissues, Peripheral Blood, and Skin Biopsies from Patients

Single-cell suspensions of tumor tissues were obtained from biopsied or autopsied (Case 1) tumor specimens that were minced mechanically and treated with collagenase and DNase. RCC cells and TILs were separated by density gradient centrifugation, as described elsewhere [24]. Heparinized peripheral blood samples (20 ml) were drawn from patients every other week before vaccination. For follow-up, samples were also drawn when the patients permitted. Patients' sera were frozen at −80°C until use for Western blot analysis. PBMC were isolated as above. PBMC and TIL (5×10^6 cells/tube) were cryopreserved using a programmable freezer and stored in liquid nitrogen. In addition, the cell pellets were frozen in liquid nitrogen until used for RNA extraction. Skin biopsies obtained from the DTH reaction site (6 mm in diameter) were cut into pieces measuring approximately 1 × 1 mm and rapidly frozen in liquid nitrogen until used for RNA extraction.

Assessment of Lymphocyte Proliferation and Cytokine Production

On the day of the assay, the cryopreserved samples were thawed. PBMC (1×10^5 cells/well) were cultured in the presence of irradiated (150 Gy) GM-CSF-transduced autologous tumor cells (1×10^4 cells/well) plus IL-2 (40 U/ml), in 96-well flat-bottomed plates. RPMI 1640 medium with L-glutamine (Invitrogen, Carlsbad, CA, USA) supplemented with 10% fetal bovine serum (BioWhittaker, Walkersville, MD, USA) and gentamicin was used as complete medium. On day 3 or 6, culture supernatants (100 μl/well) were collected from each well to determine the cytokine levels, and fresh medium was added. The cultures were then pulsed with [^{3}H]thymidine (0.5 μCi/well; DuPont-NEN, Boston, MA, USA) for a final 18 h and harvested on a Micro 96 harvester (Skatron, Lier, Norway), and the incorporated radioactivity was measured using a

microplate counter (Micro Beta Plus; Wallac, Turku, Finland). ELISAs for human IFN-γ, IL-5, and IL-10 were performed using ELISA kits (OptEIA; BD-Biosciences, Boston, MA, USA) according to the manufacturer's protocols.

Cytotoxicity Assay

To prepare effector cells, cultures with IL-2 and irradiated GM-CSF-transduced autologous tumor cells as described above were prepared in 96-well round-bottomed plates and the plates were cultured for 7 days. On the day of the assay, aliquots of 100 μl of the culture medium were removed from each well and then labeled target cells (5×10^3 cells/100 μl/well) were added. To label the target cells, single-cell suspensions of cultured autologous or allogeneic RCC cells, autologous NRC, and K562 cells were incubated with $Na_2^{51}CrO_4$ (100 μCi) for 1 h at 37°C and washed three times prior to use. For blocking experiments, F(ab′)2 anti-CD3 mAb prepared as described previously [44] was added to a final concentration of 10 μg/ml at the start of the assay. The plates were incubated at 37°C for 6 h, the supernatants were collected using a Skatron cell harvester system (Diversified Equipment Co., Lorton, VA, USA), and the radioactivity was measured using a γ counter. Spontaneous release (SR) and maximal release (MR) were measured in the supernatant of target cells alone with 100 μl of either medium or 10% Triton X-100 (Sigma, St. Louis, MO, USA). The percentage specific cytotoxicity was calculated using the following formula: % cytotoxicity = experimental release − SR/MR − SR × 100.

Analysis of the TCR β Repertoire

Total RNA was isolated from PBMC and homogenized tumor tissues using Trizol reagent (Invitrogen) with a cryo-press crusher (Microtech Nichion, Tokyo, Japan). TCR β repertoire analysis was performed as described previously [45]. Briefly, TCR β cDNA was synthesized using C-oligonucleotides (5′-CGGGCTGCTCCTT GAGGGGCTGCG-3′) with AMV reverse transcriptase (Invitrogen). The TCR cDNA was amplified by 40 cycles of PCR with each of the 24 Vβ 5′ primers (Vβ 1-w24) and the Cβ 3′ primer in PCR buffer containing 1 U of Hot Start *Taq* polymerase (AmpliTaq Gold; Applied Biosystems, Foster City, CA, USA). The products were subjected to Southern blot analysis using a ^{32}P-labeled Cβ probe. Different samples of each Vβ product were compared after quantifying the autoradiographs by densitometry BAS-2000II (Fuji Photo Film Corp.). To refine CDR3 size analysis, the Vβ–Cβ PCR product was copied in a 10-cycle run-off reaction with a fluorescence-labeled Cβ primer. The labeled PCR products were electrophoresed on a DNA sequencer (ABI Prism 377; Applied Biosystems) in the presence of a fluorescent size standard and analyzed with a DNA fragment size program (GeneScan; Applied Biosystems).

The PCR products of the CDR3 fragment were cloned into the pCRII-TOPO vector system (Invitrogen). Thirty colonies containing the insert fragment were selected at random and sequenced using an ABI Prism Cycle Sequencing Kit (Applied Biosystems) and an automatic DNA sequencer ABI 373 (Applied Biosystems). The amino acid sequence of the CDR3 region was deduced using the software GENETYX-MAC v10.1.4 (Software Development Co., Ltd., Tokyo, Japan).

Detection of Antitumor Antibodies

The antitumor antibodies appearing in patients' sera were detected by Western blot analysis according to the standard procedure with some modifications [18]. Briefly, humoral antitumor immune responses were evaluated using the reactivity of the tumor cell lysate and sera from the patients. Autologous RCC and NRC were extracted in lysis buffer containing 20 mM Tris–HCl at pH 7.6, 1% NP-40, 150 mM NaCl, 1 mM phenylmethylsulfonyl fluoride, and 500 units/ml aprotinin (Calbiochem, La Jolla, CA, USA). A fibroblast cell line of human lip origin, which was established in our laboratory, and a small-cell lung carcinoma cell line, H69, were used as irrelevant control cells. Cell lysates were denatured, reduced in SDS sample buffer with 2-mercaptoethanol, and then electrophoresed on 7.5% polyacrylamide minigels (Bio-Rad Laboratories, Hercules, CA, USA). The proteins were transferred onto Immobilon membranes (Millipore, Bedford, MA, USA) and the blots were stained with Ponceau S solution (Sigma) for visualization. After destaining with TBST (0.1% Tween 20–Tris-buffered saline) and blocking with 5% nonfat dried milk in TBST overnight, the blots were probed with diluted (1:300) patient sera for 2 h. Horseradish peroxidase-conjugated rabbit F(ab′)2 anti-IgG Ab (DAKO, 1:3000 dilution) was added for 1 h, and the blots were developed with an ECL kit (Amersham Biosciences, Piscataway, NJ, USA).

ACKNOWLEDGMENTS

We thank Drs. Fumihiko Komine, Tsuyoshi Tanabe, Hitomi Nagayama, Hitoshi Hibino, Muneomi Endo, Tomoko Yamazaki, Mariko Morishita, Koichiro Kuwabara, Momoyo Ohki, Sanae Suzuki, and the staff of The Advanced Clinical Research Center, Research Hospital, The Institute of Medical Science, University of Tokyo, for their excellent patient care and their strong support of this clinical study. We also thank Drs. Ken-ichi Tobisu and Hiroyuki Fujimoto (National Cancer Center, Japan), Taro Shuin (Kochi Medical College), Shunichi Fukuhara (Kyoto University), Yusuke Nakamura (The Institute of Medical Science, University of Tokyo), Toshio Kuroki (Gifu University), Ken-ichi Arai (The Institute of Medical Science, University of Tokyo), Jonathan W. Simons (Emory University), and Glenn Dranoff (Dana-Farber Cancer Institute) for helpful advice and discussions. This work was supported by grants from the Ministry of Health, Labor, and Welfare and the Ministry of Education, Culture, Sports, Science, and Technology, Japan.

RECEIVED FOR PUBLICATION JULY 5, 2004; ACCEPTED JULY 5, 2004.

REFERENCES

1. Marumo, K., *et al.* (2001). The prevalence of renal cell carcinoma: nation-wide survey in Japan in 1997. *Int. J. Urol.* **8:** 359–365.
2. Medical Research Council Renal Cancer Collaborators Interferon-α and survival in

doi:10.1016/j.ymthe.2004.07.001

metastatic renal carcinoma: early results of a randomized controlled trial. *Lancet* **353:** 14–17.
3. Bukowski, R. M. (1997). Natural history and therapy of metastatic renal cell carcinoma. *Cancer* **80:** 1198–1220.
4. Motzer, R. J., Bacik, J., Murphy, B. A., Russo, P., and Mazumdar, M. (2002). Interferon-α as a comparative treatment for clinical trials of new therapies against advanced renal cell carcinoma. *J. Clin. Oncol.* **20:** 289–296.
5. Clark, J. I., *et al.* (1999). Daily subcutaneous ultra-low-dose interleukin 2 with daily low-dose interferon-α in patients with advanced renal cell carcinoma. *Clin. Cancer Res.* **5:** 2374–2380.
6. Tagliaferri, P., *et al.* (1998). Daily low-dose subcutaneous recombinant interleukin-2 by alternate weekly administration. *Am. J. Clin. Oncol.* **21:** 48–53.
7. Figlin, R. A., *et al.* (1999). Multicenter, randomized, phase III trial of $CD8^+$ tumor-infiltrating lymphocytes in combination with recombinant interleukin-2 in metastatic renal cell carcinoma. *J. Clin. Oncol.* **17:** 2521–2529.
8. Childs, R., *et al.* (2000). Regression of metastatic renal-cell carcinoma after non-myeloablative allogeneic peripheral-blood stem-cell transplantation. *N. Engl. J. Med.* **343:** 750–758.
9. Dranoff, G., *et al.* (1993). Vaccination with irradiated tumor cells engineered to secrete murine granulocyte-macrophage colony-stimulating factor stimulates potent, specific, and long-lasting anti-tumor immunity. *Proc. Natl. Acad. Sci. USA* **90:** 3539–3543.
10. Jaffee, E. M., Thomas, M. C., Huang, A. Y. C., Hauda, K. M., Levitsky, H. I., and Pardoll, D. M. (1996). Enhanced immune priming with spatial distribution of paracrine cytokine vaccines. *J. Immunother.* **19:** 176–183.
11. Dranoff, G. (2002). GM-CSF-based cancer vaccines. *Immunol. Rev.* **188:** 147–154.
12. Ellem, K. A., *et al.* (1997). A case report: immune responses and clinical course of the first human use of granulocyte/macrophage-colony-stimulating-factor-transduced autologous melanoma cells for immunotherapy. *Cancer Immunol. Immunother.* **44:** 10–20.
13. Berns, A. J., *et al.* (1995). Phase I study of non-replicating autologous tumor cell injections using cells prepared with or without GM-CSF gene transduction in patients with metastatic renal cell carcinoma. *Hum. Gene Ther.* **6:** 347–368.
14. Simons, J. W., *et al.* (1997). Bioactivity of autologous irradiated renal cell carcinoma vaccines generated by ex vivo granulocyte-macrophage colony-stimulating factor gene transfer. *Cancer Res.* **57:** 1537–1546.
15. Simons, J. W., *et al.* (1999). Induction of immunity to prostate cancer antigens: results of a clinical trial of vaccination with irradiated autologous prostate tumor cells engineered to secrete granulocyte-macrophage colony-stimulating factor using ex vivo gene transfer. *Cancer Res.* **59:** 5160–5168.
16. Soiffer, R., *et al.* (1998). Vaccination with irradiated autologous melanoma cells engineered to secrete human granulocyte-macrophage colony-stimulating factor generates potent antitumor immunity in patients with metastatic melanoma. *Proc. Natl. Acad. Sci. USA* **95:** 13141–13146.
17. Chang, A. E., Li, Q., Bishop, D. K., Normolle, D. P., Redman, B. D., and Nickoloff, B. J. (2000). Immunogenic therapy of human melanoma utilizing autologous tumor cells transduced to secrete granulocyte-macrophage colony-stimulating factor. *Hum. Gene Ther.* **11:** 839–850.
18. Jaffee, E. M., *et al.* (2001). Novel allogeneic granulocyte-macrophage colony-stimulating factor-secreting tumor vaccine for pancreatic cancer: a phase I trial of safety and immune activation. *J. Clin. Oncol.* **19:** 145–156.
19. Kusumoto, M., *et al.* (2001). Phase 1 clinical trial of irradiated autologous melanoma cells adenovirally transduced with human GM-CSF gene. *Cancer Immunol. Immunother.* **50:** 373–381.
20. Salgia, R., *et al.* (2003). Vaccination with irradiated autologous tumor cells engineered to secrete granulocyte-macrophage colony-stimulating factor augments antitumor immunity in some patients with metastatic non-small-cell lung carcinoma. *J. Clin. Oncol.* **21:** 624–630.
21. Soiffer, R., *et al.* (2003). Vaccination with irradiated, autologous melanoma cells engineered to secrete granulocyte-macrophage colony-stimulating factor by adeno-viral-mediated gene transfer augments antitumor immunity in patients with metastatic melanoma. *J. Clin. Oncol.* **21:** 3343–3350.
22. Nemunaitis, J., *et al.* (2004). Granulocyte-macrophage colony-stimulating factor gene-modified autologous tumor vaccines in non-small-cell lung cancer. *J. Natl. Cancer Inst.* **96:** 326–331.
23. Tani, K., *et al.* (2000). Progress reports on immune gene therapy for stage IV renal cell carcinoma using lethally irradiated granulocyte-macrophage colony-stimulating factor-transduced autologous renal cancer cells. *Cancer Chemother. Pharmacol.* **46**(Suppl.)**:** S73–S76.
24. Kawai, K., *et al.* (2002). Advanced renal cell carcinoma treated with granulocyte-macrophage colony-stimulating factor gene therapy: a clinical course of the first Japanese experience. *Int. J. Urol.* **9:** 462–466.
25. Thomas, M. C., Greten, T. F., Pardoll, D. M., and Jaffee, E. M. (1998). Enhanced tumor protection by granulocyte-macrophage colony-stimulating factor expression at the site of an allogeneic vaccine. *Hum. Gene Ther.* **9:** 835–843.
26. Borrello, I., Sotomayor, E. M., Cooke, S., and Levitsky, H. I. (1999). A. universal granulocyte-macrophage colony-stimulating factor-producing bystander cell line for use in the formation of autologous tumor cell-based vaccines. *Hum. Gene Ther.* **10:** 1983–1991.
27. Luznik, L., *et al.* (2003). Successful therapy of metastatic cancer using tumor vaccines in mixed allogeneic bone marrow chimeras. *Blood* **101:** 1645–1652.
28. Mastrangelo, M. J., *et al.* (1999). Intratumoral recombinant GM-CSF-encoding virus as gene therapy in patients with cutaneous melanoma. *Cancer Gene Ther.* **6:** 409–422.
29. Hanada, K. -I., Yewdell, J. W., and Yang, J. C. (2004). Immune recognition of a human renal cancer antigen through post-translational protein splicing. *Nature* **427:** 252–256.
30. Puisieux, I., *et al.* (1996). Restriction of the T-cell repertoire in tumor-infiltrating lymphocytes from nine patients with renal-cell carcinoma: relevance of the CDR3 length analysis for the identification of in situ clonal T-cell expansions. *Int. J. Cancer* **66:** 201–208.
31. Gaudin, C., *et al.* (1995). In vivo local expansion of clonal T cell subpopulations in renal cell carcinoma. *Cancer Res.* **55:** 685–690.
32. Gaugler, B., *et al.* (1996). A new gene encoding for an antigen recognized by autologous cytolytic T lymphocytes on a human renal carcinoma. *Immunogenetics* **44:** 323–330.
33. Vissers, J. L. M., *et al.* (1999). The renal cell carcinoma-associated antigen G250 encodes a human leukocyte antigen (HLA)-A2.1-restricted epitope recognized by cytotoxic T lymphocytes. *Cancer Res.* **59:** 5554–5559.
34. Rosenberg, S. A., *et al.* (1987). A progress report on the treatment of 157 patients with advanced cancer using lymphokine-activated killer cells and interleukin-2 or high-dose interleukin-2 alone. *N. Engl. J. Med.* **316:** 889–895.
35. Nakazaki, Y., *et al.* (1998). Vaccine effect of granulocyte-macrophage colony-stimulating factor or CD80 gene-transduced murine leukemia/lymphoma cells and their cooperative enhancement of antitumor immunity. *Gene Ther* **5:** 1355–1362.
36. Wang, Z., Qiu, S. J., Ye, S. L., Tang, Z. Y., and Xiao, X. (2001). Combined IL-12 and GM-CSF gene therapy for murine hepatocellular carcinoma. *Cancer Gene Ther.* **8:** 751–758.
37. Van Elasas, A., Hurwitz, A. A., and Allison, J. P. (1999). Combination immunotherapy of B16 melanoma using anti-cytotoxic T lymphocyte-associated antigen 4 (CTLA-4) and granulocyte/macrophage colony-stimulating factor (GM-CSF)-producing vaccines induces rejection of subcutaneous and metastatic tumors accompanied by auto-immune depigmentation. *J. Exp. Med.* **190:** 355–366.
38. Kojima, T., *et al.* (2003). Tumor-derived Gp96 combined with GM-CSF gene-transduced tumor cells inhibit tumor growth in mice through migration and maturation of $CD11c^+$ cells. *Hum. Gene Ther.* **14:** 715–728.
39. Buzio, C., *et al.* (1997). Effectiveness of very low doses of immunotherapy in advanced renal cell cancer. *Br. J. Cancer* **76:** 541–544.
40. Lissoni, P., *et al.* (2002). Ten-year survival results in metastatic renal cell cancer patients treated with monoimmunotherapy with subcutaneous low-dose interleukin-2. *Anticancer Res.* **22:** 1061–1064.
41. Schomburg, A., *et al.* (1992). In vivo and ex vivo antitumor activity in patients receiving low-dose subcutaneous recombinant interleukin-2. *Nat. Immunol.* **11:** 133–143.
42. Sobol, R. E., *et al.* (1999). Interleukin 2 gene therapy of colorectal carcinoma with autologous irradiated tumor cells and genetically engineered fibroblasts: a phase I study. *Clin. Cancer Res.* **5:** 2359–2365.
43. Tani, K., *et al.* (1989). Implantation of fibroblasts transfected with human granulocyte colony-stimulating factor (G-CSF) cDNA into mice as a model of cytokine supplement gene therapy. *Blood* **74:** 1274–1280.
44. Azuma, M., Cayabyab, M., Buck, D., Phillips, J. H., and Lanier, L. L. (1992). CD28 interaction with B7 costimulates primary allogeneic proliferative responses and cytotoxicity mediated by small, resting T lymphocytes. *J. Exp. Med.* **175:** 353–360.
45. Hase, H., *et al.* (2000). Case report: the availability of TCR-Vβ repertoires analysis with RT-PCR methods for the early detection of pulmonary relapsed T-cell malignancy after the autologous stem cell transplantation. *Am. J. Hematol.* **64:** 124–127.

0022-5347/05/1731-0243/0
THE JOURNAL OF UROLOGY®

Vol. 173, 243–246, January 2005
Printed in U.S.A.
DOI: 10.1097/01.ju.0000141577.98902.49

DNA HYPOMETHYLATION ON PERICENTROMERIC SATELLITE REGIONS SIGNIFICANTLY CORRELATES WITH LOSS OF HETEROZYGOSITY ON CHROMOSOME 9 IN UROTHELIAL CARCINOMAS

TOHRU NAKAGAWA, YAE KANAI,* SAORI USHIJIMA, TADAICHI KITAMURA, TADAO KAKIZOE AND SETSUO HIROHASHI

From the Pathology Division, National Cancer Center Research Institute (TN, YK, SU, SH), Department of Urology, Faculty of Medicine, Tokyo University (TN, TKi) and National Cancer Center (TKa), Tokyo, Japan

ABSTRACT

Purpose: DNA methylation has important roles in genomic stability. Accordingly DNA hypomethylation on pericentromeric satellite regions may induce chromosomal instability through heterochromatin decondensation and chromosomal recombination enhancement. We elucidated the significance of aberrant DNA methylation on pericentromeric satellite regions during urothelial carcinogenesis.

Materials and Methods: We examined DNA methylation status on satellites 2 and 3 by Southern blotting and determined the allelic status of chromosome 9 using 6 microsatellite markers (D9S775, D9S925, D9S304, D9S303, D9S283 and D9S747) in 27 transitional cell carcinomas of the bladder, ureter or renal pelvis and corresponding noncancerous tissues.

Results: DNA hypomethylation on satellites 2 and 3 was detected in 2 (7%) and no (0%) noncancerous tissues, and in 11 (41%) and 12 (44%) urothelial carcinomas, respectively. DNA hypomethylation in urothelial carcinomas significantly correlated with histological grade ($p = 0.0012$ and 0.0043), invasion depth ($p = 0.0055$ and 0.0228) and morphological structure (papillary vs nodular, $p = 0.0161$ and 0.0297) for satellites 2 and 3, respectively. Loss of heterozygosity on at least 1 locus of chromosome 9 was detected in 14 urothelial carcinomas (52%). DNA hypomethylation on satellites 2 ($p = 0.0098$) and 3 ($p = 0.0034$) significantly correlated with loss of heterozygosity on chromosome 9.

Conclusions: DNA hypomethylation on pericentromeric satellite regions may participate in the development and progression of urothelial carcinomas by inducing loss of heterozygosity on chromosome 9.

KEY WORDS: urothelium; carcinoma, transitional cell; DNA methylation; chromosomal instability; loss of heterozygosity

DNA methylation has important roles in transcriptional regulation, chromatin remodeling and genomic stability.[1] Satellites 2 and 3, which are related families containing a frequent 5 bp repeat, are abundant in pericentromeric heterochromatin regions on chromosomes 1, 9 and 16, and heavily methylated in normal somatic cells.[2] DNA hypomethylation on such pericentromeric satellite regions may induce chromosomal instability through heterochromatin decondensation and chromosomal recombination enhancement.[3,4] DNA hypomethylation on satellites 2 and 3 has been reported to cause chromosomal instability, such as the formation of multiradiate chromosomes composed of chromosomes 1, 9 and 16, in ICF (immunodeficiency-chromosomal instability-facial anomalies) syndrome.[2]

In human cancers overall DNA hypomethylation accompanied by region specific hypermethylation is generally observed.[1] Aberrant DNA methylation may be involved in carcinogenesis by at least three possible mechanisms: induction of genomic instability as a result of decreased methylation level,[5–7] increased gene mutagenicity caused by deamination of 5-methylcytosine to thymine and repression of gene transcription through CpG island methylation in specific gene regulatory regions, including tumor suppressor genes.[1] For example, frequent chromosomal 1q copy gain with a pericentromeric break point has been reported in hepatocellular carcinomas showing DNA hypomethylation on satellite 2.[8]

The role of DNA hypomethylation in urothelial carcinomas is not fully understood, although aberrant hypermethylation on CpG islands around the promoter region and decreased expression of tumor suppressor genes, such as the *p16* and *E-cadherin* genes, have been reported.[9,10] In addition, loss of heterozygosity (LOH) on chromosome 9 is the most common genetic abnormality in urothelial carcinomas.[11] Consequently we focused on the clinicopathological significance of DNA hypomethylation on pericentromeric satellite regions in urothelial carcinomas and examined whether this hypomethylation is the underlying mechanism for LOH on chromosome 9 during human urothelial carcinogenesis.

MATERIALS AND METHODS

Patients and tissue samples. Paired specimens of primary urothelial carcinoma and corresponding noncancerous tissue were obtained from surgically resected specimens from 27 patients (U1 to U27) treated at National Cancer Center Hospital, Tokyo, Japan. The patients were 22 men and 5 women with a mean age ± SD of 67.6 ± 10.5 years (range 50 to 85).

Submitted for publication May 20, 2004.
Supported by a Grant-in-Aid for the Second Term Comprehensive 10-Year Strategy for Cancer Control and a Grant-in-Aid for Cancer Research from the Ministry of Health, Labor and Welfare of Japan, and a Research Resident Fellowship from the Foundation for Promotion of Cancer Research in Japan (TN).
* Correspondence: Pathology Division, National Cancer Center Research Institute, 5–1-1 Tsukiji, Chuo-ku, Tokyo 104-0045, Japan (FAX: 81–3-3248–2463; e-mail: ykanai@ncc.go.jp).

The primary tumor sites were the bladder, ureter and renal pelvis in 13, 5 and 9 patients, respectively. Based on histological examination 5 (19%), 10 (37%) and 12 (44%) tumors were classified as G1, G2 and G3–4 transitional cell carcinoma, while 11 (41%) and 16 (59%) were superficial (pTa and pT1) and invasive (pT2 to pT4), respectively.[12] Morphologically 21 tumors (78%) were papillary carcinoma and 6 (22%) were nodular carcinoma. Noncancerous specimens were obtained from the urothelium distant from the carcinoma.[13] In cases of widely spreading carcinomas in situ, as diagnosed histopathologically in preoperative biopsy specimens, the muscle layer of the bladder or the renal parenchyma was collected as noncancerous specimens since macroscopic examination cannot necessarily discriminate noncancerous urothelium from carcinoma in situ.

Southern blotting for pericentromeric satellite regions. High molecular weight DNA was isolated from fresh tissue samples by phenol-chloroform extraction and dialysis. DNA methylation status was assessed by digesting DNA with *Msp* I and *Hpa* II, which cut at the sequence CCGG. *Hpa* II does not cut when the internal cytosine is methylated. High molecular weight DNA (5 μg) was digested for 24 hours with 10 U *Msp* I or *Hpa* II/μg DNA. DNA fragments were separated by electrophoresis, transferred to nitrocellulose membranes and hybridized with ^{32}P labeled DNA probes. Previously described oligonucleotides were used as probes for satellites 2 and 3.[14]

Analysis of LOH on chromosome 9. Genomic DNA was amplified by polymerase chain reaction (PCR) using oligonucleotide primers for 6 microsatellite loci on chromosome 9, namely D9S775, D9S925, D9S304, D9S303, D9S283 and D9S747. Primer sequences were D9S775 (9p23) 5′-AAAGTAGCCATCCGTGTGT-3′ and 5′-GCTTTCTTTGATGGTTTACAG-3′, D9S925 (9p21–22) 5′-GTCTGGGTTCTCCAAAGAAA-3′ and 5′-TGTGAGCCAAGGCCTTATAG-3′, D9S304 (9p21) 5′-GTGCACCTCTACACCCAGAC-3′ and 5′-TGTGCCCACACACATCTATC-3′, D9S303 (9q21) 5′-CAACAAAGCAAGATCCCTTC-3′ and 5′-TAGGTACTTGGAAACTCTTGGC-3′, D9S283 (9q22) 5′-TGCTGGATTTCAGGTAGGG-3′ and 5′-ATGGTTATGCGGGTGTATTTCTC-3′, and D9S747 (9q32) 5′-GCCATTATTGACTCTGGAAAAGAC-3′ and 5′-CAGGCTCTCAAAATATGAACAAAAT-3′. The 5′ ends of forward primers were labeled with 6-carboxyfluorescein and PCR amplifications were performed with 20 ng genomic DNA. Subsequently PCR products were fractionated by electrophoresis (ABI 3100 sequencer, Applied Biosystems, Foster City, California) according to the manufacturer protocol. Data were analyzed with the GeneScan, version 3.7 computer program (Applied Biosystems). When 2 amplified bands per locus were detected in the noncancerous tissue specimen, the case was considered informative for LOH analysis. LOH was recorded when signal intensity for a tumor allele was decreased by more than 50% relative to the matched normal allele in informative cases, as described previously.[15–17] Replication error was identified by the presence of band shifts or the presence of novel bands in PCR products.

Statistics. Correlations between any 2 of DNA methylation status, allelic status and clinicopathological parameters were analyzed by the chi-square test with $p < 0.05$ considered significant.

RESULTS

DNA methylation status on pericentromeric satellite regions and its correlation with clinicopathological parameters. Figure 1 shows examples of Southern blotting. In 25 (93%) and all 27 (100%) noncancerous tissue specimens examined significantly larger DNA fragments were detected in *Hpa* II digests compared with *Msp* I digests at satellites 2 and 3, respectively, indicating that these regions were heavily methylated. In 11 (41%) and 12 (44%) urothelial carcinomas smaller fragments were detected in *Hpa* II digest compared with corresponding normal tissues or *Hpa* II digest showed almost the same hybridization pattern as the *Msp* I digest of the same sample and the corresponding normal tissue, indicating that these regions were hypomethylated. In almost all carcinoma samples in which DNA hypomethylation was detected hypomethylation occurred on satellites 2 and 3.

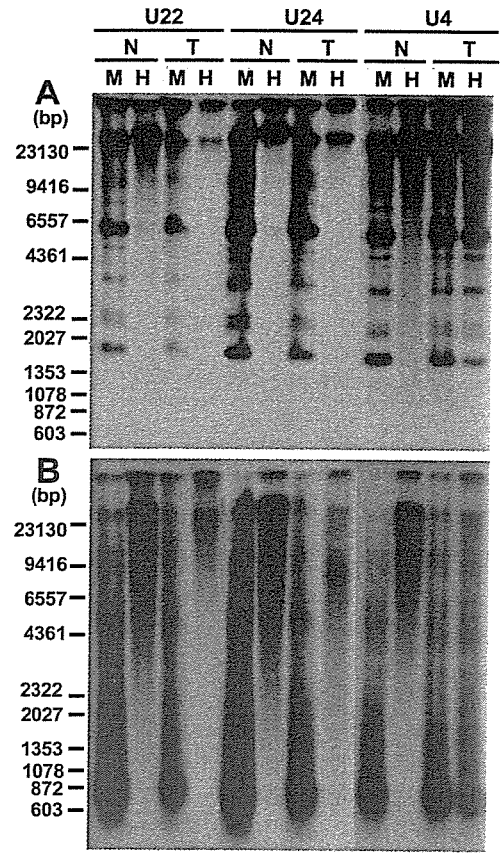

FIG. 1. Examples of Southern blotting for satellites 2 (*A*) and 3 (*B*) in cases of urothelial carcinoma. Methylation status was assessed by digesting DNA with *Msp* I (*Lane M*) and *Hpa* II (*Lane H*). DNA fragments were separated by electrophoresis, transferred to nitrocellulose membranes and hybridized with ^{32}P labeled DNA probes. Larger bands were detected in lane H compared with lane M in all noncancerous tissue (*N*), and in U22T and U24T, indicating that satellite 2 region was heavily methylated (*A*). In U4T lane H showed same hybridization pattern as lane M, indicating that this region was hypomethylated. (*B*) In all noncancerous tissues, and U22T and U24T satellite 3 region was heavily methylated, whereas this region was hypomethylated in U4T. *T*, cancerous tissue.

DNA hypomethylation on pericentromeric satellite regions significantly correlated with histological grade (chi-square test $p = 0.0012$ and 0.0043), invasion depth (chi-square test $p = 0.0055$ and 0.0228) and morphological structure (papillary vs nodular chi-square test $p = 0.0161$ and 0.0297) for satellites 2 and 3, respectively (table 1), but not with age or gender (data not shown).

Allelic status of chromosome 9 and its correlation with clinicopathological parameters. Figure 2 shows examples of electropherograms of PCR products. Figure 3 shows the results of LOH analysis. Table 2 lists the incidence of LOH on each locus. LOH for at least 1 marker was found in 14 of the 27 informative cases (52%) (table 2).

The presence of LOH on at least 1 locus on chromosome 9 significantly correlated with histological grade (chi-square test $p = 0.0313$, table 3). LOH on at least 1 locus was detected in all 6 nodular carcinomas and its incidence (100%) was significantly higher than in papillary carcinomas (chi-square test $p = 0.0074$, table 3).

Correlation between DNA methylation status on pericentromeric satellite regions and allelic status of chromosome 9. DNA

TABLE 1. *DNA hypomethylation on pericentromeric satellite regions and clinicopathological parameters in urothelial carcinomas*

Tissue Specimens	No. Analyzed	No. Hypomethylation (%)	p Value (chi-square test)
		Satellite 2	
Histological grade:			
G1–2	15	2 (13)	
G3–4	12	9 (75)	0.0012
Invasion depth:			
Superficial (pTa, pT1)	11	1 (9)	
Invasive (pT2–4)	16	10 (63)	0.0055
Histological structure:			
Papillary	21	6 (29)	
Nodular	6	5 (83)	0.0161
		Satellite 3	
Histological grade:			
G1–2	15	3 (20)	
G3–4	12	9 (75)	0.0043
Invasion depth:			
Superficial (pTa, pT1)	11	2 (18)	
Invasive (pT2–4)	16	10 (63)	0.0228
Histological structure:			
Papillary	21	7 (33)	
Nodular	6	5 (83)	0.0297

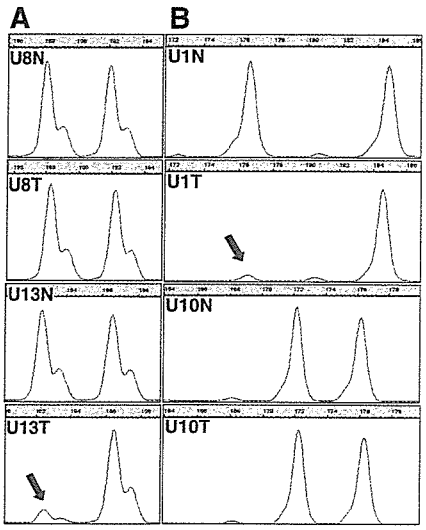

FIG. 2. Examples of results of allelic status analyses in cases of urothelial carcinoma. U8 and U13 DNA samples were amplified for D9S747 (*A*), while U1 and U10 samples were amplified for D9S775 (*B*). Genotypes derived from noncancerous U8N, U13N, U1N and U10N tissues, and corresponding U8T, U13T, U1T and U10T cancerous tissues are shown. Allele size in bp is indicated on top of horizontal axis. In all 4 noncancerous samples PCR products showed polymorphism, indicating that these cases were informative. U8T for D9S747 and U10T for D9S775 were classified as retention of alleles because signal intensity for tumor alleles was not changed significantly relative to matched normal alleles. LOH was identified when signal intensity for tumor allele was decreased by more than 50% relative to matched normal allele, that is in U13T for D9S747 and U1T for D9S775 (arrows).

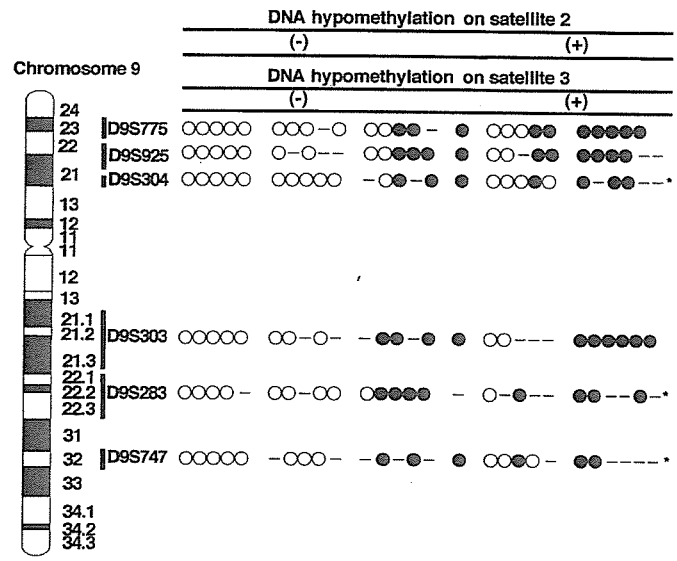

FIG. 3. Allelic status of each locus in urothelial carcinomas. Vertical lines indicate each carcinoma. Open circles indicate retention of 2 alleles. Filled circle indicate LOH. Bar indicates uninformative case. Asterisk indicates replication error. −, negative. +, positive.

TABLE 2. *LOH on chromosome 9 in urothelial carcinomas*

Locus	No. Analyzed	No. Informative	No. LOH (%)
9p:			
D9S775	27	24	10 (42)
D9S925	27	21	10 (48)
D9S304	27	22	7 (32)
Any on 9p	27	26	11 (42)
9q:			
D9S303	27	20	10 (50)
D9S283	27	18	8 (44)
D9S747	27	17	6 (35)
Any on 9q	27	26	12 (46)
Any on chromosome 9	27	27	14 (52)

hypomethylation on pericentromeric satellite regions significantly correlated with the presence of LOH on at least 1 locus on chromosome 9 in urothelial carcinomas (chi-square test p = 0.0098 and 0.0034 for satellites 2 and 3, respectively, table 4).

DISCUSSION

DNA hypomethylation on satellites 2 and 3 was observed frequently in urothelial carcinomas but it was extremely rare in noncancerous tissues, suggesting that DNA hypomethylation on satellites 2 and 3 is associated with urothelial carcinogenesis. We have previously reported that DNA hypomethylation on satellites 2 and 3 is a frequent and early event during hepatocarcinogenesis,[18] whereas it is rare in colorectal and stomach cancers.[19] These and the current findings suggest that DNA hypomethylation on pericentromeric satellite regions is organ specific during human carcinogenesis. In the current study DNA hypomethylation correlated with tumor aggressiveness (eg histological grade and invasion depth), indicating that it may participate in the malignant progression of urothelial carcinomas. In addition, DNA hy-

TABLE 3. *LOH on chromosome 9 and clinicopathological parameters in urothelial carcinomas*

Parameters	No. Analyzed	No. LOH (%)	p Value (chi-square test)
Histological grade:			
G1–2	15	5 (33)	
G3–4	12	9 (75)	0.0313
Invasion depth:			
Superficial (pTa, pT1)	11	4 (36)	
Invasive (pT2–4)	16	10 (63)	0.1817
Histological structure:			
Papillary	21	8 (38)	
Nodular	6	6 (100)	0.0074

TABLE 4. *DNA hypomethylation on pericentromeric satellite regions and LOH on chromosome 9 in urothelial carcinomas*

Chromosome 9 LOH	Hypomethylation		p Value (chi-square test)
	Neg	Pos	
Satellite 2:			
Neg	11	2	
Pos	5	9	0.0098
Satellite 3:			
Neg	11	2	
Pos	4	10	0.0034

pomethylation was associated more frequently with nodular invasive carcinomas showing an aggressive clinical outcome than with papillary carcinomas. Nodular invasive carcinomas arise from their precursor lesions, that is widely spreading flat carcinoma in situ, and rapidly invading suburothelial tissues, whereas papillary carcinomas usually remain noninvasive for a long period, even after recurrence in the bladder following cystoscopic resection.[13]

LOH on chromosome 9 was detected in more than half of the cases and in these cases rather large regions of 9p and/or 9q were lost, consistent with other reports that loss of an entire chromosome arm is frequent (fig. 3).[11] The observed high incidence of LOH on chromosome 9 in urothelial carcinomas may indicate the existence of tumor suppressor genes important for urothelial carcinogenesis on this chromosome.[11] DNA hypomethylation on satellites 2 and 3 significantly correlated with LOH on chromosome 9 in urothelial carcinomas. After the induction of DNA hypomethylation in cultured cells by treatment with 5-azacytidine, a DNA methyltransferase inhibitor, chromosomal recombination occurred between satellite regions.[3] In patients with ICF syndrome DNA hypomethylation on satellites 2 and 3, and multiradiate chromosomes composed of chromosomes 1, 9 and 16 are characteristic.[2] During hepatocarcinogenesis DNA hypomethylation on satellite 2 significantly correlates with chromosome 1 q-arm copy gain with pericentromeric break points.[8] By analogy with these findings DNA hypomethylation on satellites 2 and 3 could be the underlying molecular background for the frequently observed LOH on chromosome 9 in urothelial carcinomas.

DNMT3b has been identified as a DNA methyltransferase specifically targeting satellites 2 and 3 during mouse development.[20] In human hepatocarcinogenesis over expression of DNMT3b4, a splice variant of DNMT3b that lacks methyltransferase activity and competes with the major variant in normal liver tissues, DNMT3b3, for targeting to pericentromeric satellite regions, results in DNA hypomethylation on these regions.[21] Although further studies are needed to understand the molecular mechanism causing DNA hypomethylation on satellites 2 and 3 during urothelial carcinogenesis, this hypomethylation may have a role in the development and progression of urothelial carcinomas by inducing chromosomal instability. These data highlight the practical significance of correction of DNA methylation status for the prevention and/or therapy of urothelial carcinomas.

REFERENCES

1. Jones, P. A. and Baylin, S. B.: The fundamental role of epigenetic events in cancer. Nat Rev Genet, **3:** 415, 2002
2. Xu, G. L., Bestor, T. H., Bourc'his, D., Hsieh, C. L., Tommerup, N., Bugge, M. et al: Chromosome instability and immunodeficiency syndrome caused by mutations in a DNA methyltransferase gene. Nature, **402:** 187, 1999
3. Kokalj-Vokac, N., Almeida, A., Viegas-Pequignot, E., Jeanpierre, M., Malfoy, B. and Dutrillaux, B.: Specific induction of uncoiling and recombination by azacytidine in classical satellite-containing constitutive heterochromatin. Cytogenet Cell Genet, **63:** 11, 1993
4. Suzuki, T., Fujii, M. and Ayusawa, D.: Demethylation of classical satellite 2 and 3 DNA with chromosomal instability in senescent human fibroblasts. Exp Gerontol, **37:** 1005, 2002
5. Chen, R. Z., Pettersson, U., Beard, C., Jackson-Grusby, L. and Jaenisch, R.: DNA hypomethylation leads to elevated mutation rates. Nature, **395:** 89, 1998
6. Gaudet, F., Hodgson, J. G., Eden, A., Jackson-Grusby, L., Dausman, J., Gray, J. W. et al: Induction of tumors in mice by genomic hypomethylation. Science, **300:** 489, 2003
7. Eden, A., Gaudet, F., Waghmare, A. and Jaenisch, R.: Chromosomal instability and tumors promoted by DNA hypomethylation. Science, **300:** 455, 2003
8. Wong, N., Lam, W. C., Lai, P. B., Pang, E., Lau, W. Y. and Johnson, P. J.: Hypomethylation of chromosome 1 heterochromatin DNA correlates with q-arm copy gain in human hepatocellular carcinoma. Am J Pathol, **159:** 465, 2001
9. Maruyama, R., Toyooka, S., Toyooka, K. O., Harada, K., Virmani, A. K., Zochbauer-Muller, S. et al: Aberrant promoter methylation profile of bladder cancer and its relationship to clinicopathological features. Cancer Res, **61:** 8659, 2001
10. Bornman, D. M., Mathew, S., Alsruhe, J., Herman, J. G. and Gabrielson, E.: Methylation of the E-cadherin gene in bladder neoplasia and in normal urothelial epithelium from elderly individuals. Am J Pathol, **159:** 831, 2001
11. Knowles, M. A.: The genetics of transitional cell carcinoma: progress and potential clinical application. BJU Int, **84:** 412, 1999
12. Sobin, L. H. and Wittekind, Ch.: TNM Classification of Malignant Tumors, 5th ed. New York: John Wiley & Sons, Inc., 1997
13. Friedell, G. H., Parija, G. C., Nagy, G. K. and Soto, E. A.: The pathology of human bladder cancer. Cancer, **45:** 1823, 1980
14. Tagarro, I., Fernandez-Peralta, A. M. and Gonzalez-Aguilera, J. J.: Chromosomal localization of human satellites 2 and 3 by a FISH method using oligonucleotides as probes. Hum Genet, **93:** 383, 1994
15. Hartmann, A., Rosner, U., Schlake, G., Dietmaier, W., Zaak, D., Hofstaedter, F. et al: Clonality and genetic divergence in multifocal low-grade superficial urothelial carcinoma as determined by chromosome 9 and p53 deletion analysis. Lab Invest, **80:** 709, 2000
16. Hartmann, A., Schlake, G., Zaak, D., Hungerhuber, E., Hofstetter, A., Hofstaedter, F. et al: Occurrence of chromosome 9 and p53 alterations in multifocal dysplasia and carcinoma in situ of human urinary bladder. Cancer Res, **62:** 809, 2002
17. Obermann, E. C., Junker, K., Stoehr, R., Dietmaier, W., Zaak, D., Schubert, J. et al: Frequent genetic alterations in flat urothelial hyperplasias and concomitant papillary bladder cancer as detected by CGH, LOH, and FISH analyses. J Pathol, **199:** 50, 2003
18. Saito, Y., Kanai, Y., Sakamoto, M., Saito, H., Ishii, H. and Hirohashi, S.: Expression of mRNA for DNA methyltransferases and methyl-CpG-binding proteins and DNA methylation status on CpG islands and pericentromeric satellite regions during human hepatocarcinogenesis. Hepatology, **33:** 561, 2001
19. Kanai, Y., Ushijima, S., Kondo, Y., Nakanishi, Y. and Hirohashi, S.: DNA methyltransferase expression and DNA methylation of CPG islands and peri-centromeric satellite regions in human colorectal and stomach cancers. Int J Cancer, **91:** 205, 2001
20. Okano, M., Bell, D. W., Haber, D. A. and Li, E.: DNA methyltransferases Dnmt3a and Dnmt3b are essential for de novo methylation and mammalian development. Cell, **99:** 247, 1999
21. Saito, Y., Kanai, Y., Sakamoto, M., Saito, H., Ishii, H. and Hirohashi, S.: Overexpression of a splice variant of DNA methyltransferase 3b, DNMT3b4, associated with DNA hypomethylation on pericentromeric satellite regions during human hepatocarcinogenesis. Proc Natl Acad Sci USA, **99:** 10060, 2002

Reprinted from
Jpn J Clin Oncol 2004;34(3)118–123

Magnetic Anchor for More Effective Endoscopic Mucosal Resection

Toshiaki Kobayashi[1], Takushi Gotohda[1], Katsunori Tamakawa[2], Hirohisa Ueda[3] and Tadao Kakizoe[1]

[1]National Cancer Center, Tokyo, [2]Tamakawa Corporation, Sendai, [3]Pentax Corporation, Tokyo, Japan